Heart Slice Culture System Reliably Demonstrates Clinical Drug-Related Cardiotoxicity

Jessica M. Miller*[1,2]; Moustafa H. Meki*[1,2]; Qinghui Ou*[1]; Sharon A. George*[3]; Anna Gams[3]; Riham R. E. Abouleisa[1]; Xian-Liang Tang[1]; Brooke M. Ahern[4]; Guruprasad A. Giridharan[2]; Ayman El-Baz[2]; Bradford G. Hill[5]; Jonathan Satin[4]; Daniel J. Conklin[5]; Javid Moslehi[6]; Roberto Bolli[1]; Alexandre J. S. Ribeiro[7]; Igor R. Efimov[3]; Tamer M. A. Mohamed[1,2,5,8,9,10].

[1]From the Institute of Molecular Cardiology, Department of Medicine, University of Louisville, KY, USA

[2]Department of Bioengineering, University of Louisville, KY, USA

[3]Department of Biomedical Engineering, The George Washington University, Washington, DC, USA

[4]Department of Physiology, University of Kentucky, KY, USA

[5]Envirome Institute, Diabetes and Obesity Center, Department of Medicine, University of Louisville, KY, USA

[6] Division of Cardiology, Cardio-Oncology Program, Vanderbilt University Medical Center, 2220 Pierce Avenue, Nashville, USA.

[7]U.S. Food and Drug Administration, Center for Drug Evaluation and Research, Office of Translational Science, Office of Clinical Pharmacology, Division of Applied Regulatory Science, Silver Spring, MD, USA

[8]Department of Pharmacology and Toxicology, University of Louisville, KY, USA

[9]Institute of Cardiovascular Sciences, University of Manchester, UK

[10]Faculty of Pharmacy, Zagazig University, Egypt

* Authors equally contributed to the work.

Correspondence to:

Tamer M A Mohamed, Institute of Molecular Cardiology, University of Louisville, 580 South Preston Street, Louisville, KY 40202. Email: tamer.mohamed@louisville.edu

Igor R Efimov, Department of Biomedical Engineering, The George Washington University, 5000 Science and Engineering Hall, Washington, DC 20052, USA. Email: efimov@gwu.edu

Alexandre J. S. Ribeiro, U.S. Food and Drug Administration, Center for Drug Evaluation and Research, Office of Translational Science, Office of Clinical Pharmacology, Division of Applied Regulatory Science, Silver Spring, MD, USA. Email: Alexandre.Ribeiro@fda.hhs.gov

Abstract

The limited availability of human heart tissue and its complex cell composition are major limiting factors for reliable testing drug efficacy, toxicity and understanding mechanism. Recently, we developed a functional human and pig heart slice biomimetic culture system that fully preserves the viability and functionality of 300 μm heart slices for 6 days. Here, we tested the reliability of this culture system in delineating the mechanisms of known anti-cancer drugs that cause cardiomyopathy. We tested three anti-cancer drugs (doxorubicin, trastuzumab, and sunitinib) associated with different mechanisms leading to cardiotoxicity at three concentrations and assessed the effect of these drugs on heart slice viability, structure, function and transcriptome. Slices incubated with any of these drugs for 48 h showed significant loss in viability, cardiomyocyte structure and functionality. Mechanistically, RNA sequencing demonstrated a significant downregulation of cardiac genes and upregulation of oxidative response in doxorubicin-treated tissues. Trastuzumab treatment caused major downregulation in cardiac muscle contraction-related genes, consistent with its clinically known direct effect on cardiomyocytes. Interestingly, sunitinib treatment resulted in significant downregulation of angiogenesis-related genes in line with its mechanism of action. Heart slices are not only able to demonstrate the expected toxicity of doxorubicin and trastuzumab similar to hiPS-derived-cardiomyocytes; they are superior in detecting sunitinib cardiotoxicity phenotypes and mechanism in the clinically relevant concentration range, 100 nM – 1 μM. These results indicate that heart slice tissue culture models have the potential to become a reliable platform for testing drug toxicity and mechanism of action.

55 **Introduction**

56 In the past 30 years, cardiotoxicity induced by side effects of drugs that affect the electrical
57 activity as well as the contractility of cardiomyocytes has been the cause for 40% of all drug
58 withdrawals from the market[1, 2]. In addition, in the last decade, there has been an explosion of
59 cancer therapies, several of which often lead to cardiotoxic effects, causing cardiomyopathy,
60 arrhythmias, irreversible heart failure or death[3]. For example, both traditional (e.g.,
61 anthracyclines and radiation) and targeted (e.g., trastuzumab) breast cancer therapies can
62 result in cardiovascular complications in a subset of patients[4, 5]. The cardiovascular effects of
63 newer classes of drugs, such as CDK4/6 inhibitors and PI3K inhibitors, are still unclear[6, 7]. The
64 recent higher cancer survival is partially offset by increased morbidity and mortality related to
65 the cardiotoxic side effects of anti-cancer therapeutics[8]. Hence, a close collaboration between
66 cardiologists and oncologists (in the emerging field of cardio-oncology) aims to make these
67 complications manageable to ensure that patients can be treated as safely and as effectively as
68 possible[2].

69 Detection of cardiotoxic effects of drug candidates requires the use of *in vivo* and *in vitro*
70 studies prior to clinical trials[9]. Therefore, there is a growing need for reliable preclinical screening
71 strategies for cardiovascular toxicities associated with emerging cancer therapies prior to human
72 clinical trials. Animal models can fail in predicting drug adverse cardiac effects[10, 11], can be
73 expensive and do not replicate many of the biochemical properties and hemodynamic aspects of
74 the human heart and circulation[12-14]. Recently, human induced pluripotent stem cell derived
75 cardiomyocytes (hiPSC-CMs) started being used to assess cardiotoxicity[15, 16]. However, these
76 cells have several fetal-like properties that can limit their usefulness in comprehensively predicting
77 clinical cardiac drug side effects. The development of hiPSC-CMs microtissues is a promising
78 effort to generate more mature phenotypes, but it is still a work in progress[15, 16]; because such
79 microtissues still exhibit immature electrophysiology and lack cell-cell electrical coupling[17]. A less

common approach has been the use of isolated primary human cardiomyocytes. While these cells are functionally mature, and can be used for high-throughput testing, they readily dedifferentiate in culture, thereby limiting their use for cardiotoxicity studies[18]. The adult human heart tissue is structurally more complicated, being composed of a heterogeneous mixture of various cell types including cardiomyocytes, endothelial cells, smooth muscle cells, and various types of stromal fibroblasts linked together with a sophisticated three-dimensional network of extracellular matrix proteins[19]. This heterogeneity of the non-cardiomyocyte cell population[20-22] in the adult heart is a major obstacle in modeling heart tissue using individual cell types. Human ventricular wedge preparations have also been used to study electrophysiology[23, 24]. However, the wedge preparations are typically large in size and have functional viability of only several hours, limiting their applicability to high-throughput applications.

These major limitations highlight the importance of developing optimal methods to enable the culture of intact cardiac tissue for studies involving physiological and pathological conditions[17]. Culturing human heart slices has shown promise in extending the functionality and viability of cardiac tissue. By retaining the normal tissue architecture, the multi-cell type environment, and the 3-dimensional structure, tissue slices can more faithfully replicate the organ-level adult cardiac physiology in terms of normal conduction velocity, action potential duration, and intracellular calcium dynamics[25, 26]. Recently, we have developed a novel biomimetic culture system that maintains full viability and functionality of human and pig heart slices (300 μm thickness) for 6 days in culture through optimization of the medium and culture conditions with continuous electrical stimulation at 1.2 Hz and oxygenation of the culture medium[27]. In the present study, we aim to test the reliability of this culture system in recapitulating clinical toxicity and potentially delineating the mechanisms of known cardiotoxic drugs. To this end, we selected three anticancer drugs with known adverse cardiac side effects: doxorubicin, an anthracycline with a long history of cardiotoxicity; trastuzumab, a monoclonal antibody target HER2; and, sunitinib, a small molecule multi-targeted kinase inhibitor (TKI) with

106 potent activity against VEGF and PDGF receptors[5]. All three drugs have been associated with
107 cardiomyopathy through a different mechanisms[5]. These 3 drugs were selected as in hiPSC-
108 CMs doxorubicin and trastuzumab are shown to be cardiotoxic[28, 29], however, nanomolar
109 concentrations of sunitinib do not cause any cardiotoxicity on hiPSC-CMs [30]. Therefore, we first
110 confirmed in our hands the previously reported data that hiPSC-CMs are able to demonstrate
111 the cardiotoxic phenotype of doxorubicin, but not sunitinib, at low concentrations[30]. Then, in pig
112 heart slices, we tested three different concentrations of each drug in ten-fold incremental values
113 with the lowest dose being the most clinically relevant and assessed the effect of these drugs on
114 heart slice viability, structure, function and transcriptome. As the maximum blood concentration
115 of doxorubicin ranges between 100nM-300nM[31], we used 100nM, 1μM, 10μM concentrations.
116 We used 1μg/mL, 10μg/mL and 100μg/mL concentrations for trastuzumab as the blood level is
117 ranging between 1-10μg/mL[32]. Sunitinib concentrations of 100nM, 1μM, 10μM were used as the
118 normal blood concentration range is 100nM-200nM[33]. Finally, we assessed the ability and
119 reproducibility of the human heart slices in demonstrating the true cardiotoxic mechanism of
120 doxorubicin between different human subjects.

121 **Methods**

122 **Apoptotic assay on hiPSC-CMs:** hiPSC-CMs (iCell Cardiomyocytes[2]) were purchased
123 from Cellular Dynamics (Currently FujiFilm Inc.). These hiPSC-CMs have been selected after
124 differentiation using an a-MHC-Blastocidin selection cassette. This strategy yields nearly 100%
125 pure hiPSC-CMs. Following vendor recommendations, hiPSC-CMs were seeded on fibronectin
126 coated plates and cultured in maintenance medium. . hiPSC-CMs were exposed to a range of
127 concentrations of doxorubicin (cardiotoxin), sunitinib (cardiotoxic TKI), aspirin (non-toxic drug),
128 erlotinib (non-cardiotoxic TKI) over 48 h. DMSO in the medium at a concentration of 0.1% (v/v)
129 was used as a control condition for each drug. Live cell brightfield and fluorescent images for
130 time-lapse experiments were acquired using the Incucyte® S3 Live Cell Analysis System

131 (Essen Bioscience / Sartorius) running version 2019A (20191.1.6976.19779). Plates were
132 imaged hourly following initiation of drug treatment. Three images at set locations within each
133 well were acquired at 10x magnification for each time point. For fluorescent imaging of
134 apoptosis, the Incucyte Caspase-3/7 Green dye (Essen Bioscience 4440) was added to the
135 media/drug cocktail at a concentration of 5 μM for the duration of the assay. Analysis of
136 apoptosis using the Caspase 3/7 fluorescent dye was performed using the Incucyte software.
137 Parameters were set to quantify green fluorescent intensity metrics and areas of high signal
138 intensity are marking cell death.

139 **Harvesting porcine heart tissue:** All animal procedures were in accordance with the
140 institutional guidelines and approved by the University of Louisville Institutional Animal Care and
141 Use Committee. The protocol for harvesting pig hearts has been described in detail[27, 34]. Briefly,
142 following deeply anesthetizing the pig with 5% isoflurane, pig heart was quickly excised out and
143 the heart was clamped at the aortic arch and perfused with 1L sterile cardioplegia solution (110
144 mM NaCl, 1.2 mM $CaCl_2$, 16 mM KCl, 16 mM $MgCl_2$, 10 mM $NaHCO_3$, 5 units/mL heparin, pH to
145 7.4), then the heart was preserved on an ice-cold cardioplegic solution and immediately
146 transported to the lab on wet ice.

147 **Human heart Slices:** Donor hearts that were not used in transplantation were acquired
148 through our collaboration with the Washington Regional Transplant Community. Human cardiac
149 organotypic slices were prepared as previously described[35, 36].

150 **Heart slicing and culturing:** Slicing and culturing 300 μm thick heart tissue slices were
151 performed as previously described in[27, 34]. A refined oxygenated growth medium was used
152 (Medium 199, 1x ITS supplement, 10% FBS, 5 ng/mL VEGF, 10 ng/mL FGF-basic, and 2x
153 Antibiotic-Antimycotic), and changed 3 times/day. Sunitinib (Tocris Inc.) (100 nM, 1μM, and 10
154 μM), trastuzumab (InvivoGen Inc.) (1 μg, 10 μg, and 100 μg), or doxorubicin (Sigma Millipore
155 Inc.) (100 nM, 1μM, and 10 μM, and 50 μM) was added freshly to the culture medium at each

156 medium change. Control slices received DMSO at the same dilution factor as the drug-treated
157 slices.

158 **MTT viability assay:** For the MTT assay we used the Vybrant ® MTT Cell Proliferation
159 Assay kit (Thermo Scientific) following the manufacturer's protocol with slight modifications.
160 Using a sterile scalpel, each heart slice was cut into 2 ~0.5 cm^2-sized sections for the MTT
161 assay. The heart slice segments were placed into a single well of a 12-well plate containing 0.9
162 mL growth media with 0.1 mL of reconstituted MTT substrate that was prepared according to
163 the manufacturer's protocol. The tissue was incubated at 37°C for 3 h. During this time, viable
164 tissue metabolized the MTT substrate and produced a purple color formazan compound. To
165 extract the purple formazan from the tissue slices, the tissue was transferred into 1 mL of
166 DMSO and incubated at 37°C for 15 min. The resulting solution was purple in color. This
167 solution was then transferred into a clear bottom 96-well plate in triplicate at 3 dilutions, 1:2, 1:5,
168 and 1:10. The intensity of the purple color was measured using cytation 1 plate reader (BioTek)
169 at 570 nm. The readings were normalized to the weight of each heart tissue section and
170 converted into OD/mg tissue. The 3 dilutions of the solution were performed to correct for any
171 possible signal saturation and the average of all readings was normalized to their dilution factor.

172 **Heart slice fixation, mounting and immunofluorescence:** Heart slices were fixed with 4%
173 paraformaldehyde for 48 h. Fixed tissue was dehydrated in 10% sucrose for 1 hour, 20%
174 sucrose for 1 h, and 30% for overnight. The dehydrated tissue was then embedded in optimal
175 cutting temperature compound (OCT compound) and gradually frozen in isopentane/dry ice
176 bath. OCT embedded blocks were stored at -80°C until sectioning. 8 μm sections were cut and
177 immunolabeled for target proteins using the following procedure: To remove the OCT
178 compound, the slides were heated for 5 min at 95°C until the OCT compound melted. Then 1
179 mL of PBS was added to each slide and incubated at RT for 10-30 min until the OCT compound
180 washed off. Sections were then permeabilized by incubating for 30 min in 0.1% Triton-X in PBS

181 at RT. The Triton-X was removed, and non-specific antibody binding of the sections were
182 blocked with 3% BSA solution for 1 h at RT. After washing the BSA off with PBS, each section
183 was marked off with a wax pen. After marking sections off, the primary antibodies (1:200 dilution
184 in 1% BSA) connexin 43 (Abcam; #AB11370), troponin-T (Thermo Scientific; #MA5-12960)]
185 were added to each section and incubated for 90 min at RT. The primary antibodies were
186 washed off with PBS three times followed by the addition of the secondary antibodies (1:200
187 dilution in 1% BSA) anti-Ms AlexaFluor 488 (Thermo Scientific; #A16079), anti-Rb AlexaFluor
188 594 (Thermo Scientific; #T6391) and incubated for 90 min at RT. The secondary antibody was
189 removed by washing the sections 3 times with PBS. To distinguish the *bona fide* target staining
190 from the background, we used a secondary antibody only as a control. After 3 times PBS
191 washes, DAPI was added for 15 min. The sections were washed again 3 times with PBS.
192 Finally, slices were mounted in vectashield (Vector Laboratories) and sealed with nail polish. All
193 immunofluorescence imaging and quantification were performed using a Cytation 1 high content
194 imager and the fluorescent signal quantification and masking were performed using the Gen5
195 software.

196 **Calcium-transient assessment:** Calcium transients were assessed as previously
197 described[27]. Briefly, heart slices were loaded with Fluo-4 for 30 min at room temperature before
198 being transferred to the imaging chamber. The loading solution contained a 1:10 mixture of
199 5 mM Fluo-4 AM in dry DMSO and PowerloadTM concentrate (Invitrogen), which was diluted
200 100-fold into extracellular Tyrode's solution (NaCl 140mM; KCl 4.5mM; glucose 10mM; HEPES
201 10mM; $MgCl_2$ 1mM; $CaCl_2$ 1.8mM; 2x Antibiotic-Antimycotic; pH 7.4). Additional 20 min were
202 allowed for de-esterification before recordings were taken. Contractions and calcium transients
203 were evoked by applying voltage pulses at 1 Hz between platinum wires placed on either side of
204 the heart slice and connected to a field stimulator (IonOptix, Myopacer). Fluo-4 fluorescence
205 transients were recorded via a standard filter set (#49011 ET, Chroma Technology). Resting

206 fluorescence was recorded after cessation of pacing, and background light was obtained after
207 removing the heart slice from the field of view at the end of the experiment. All analyses of
208 calcium transients were based on calcium transients recorded from single cardiomyocytes
209 within the heart slice and the calcium transient's amplitude was assessed as the average of 10
210 consecutive beats from each cell. Calcium transients and amplitude was assessed following
211 normalization to the basal florescence of each cell and represented as F/F_0.

212 **RNA Sequencing:** RNA was isolated from the heart slices by using the Qiagen miRNeasy
213 Micro Kit, #210874, following the manufacturer's protocol after homogenization of tissue in
214 Trizol. RNAseq library preparation, sequencing, and data analysis were performed as described
215 previously[27].

216 **Optical Mapping:** Slices were incubated with Di-4-ANEPPS (30 µl of stock solution at 1.25
217 mg/mL diluted to 1 mL with recovery solution(140 mM NaCl, 4.5 mM KCl, 1 mM MgCl2, 1.8 mM
218 CaCl2, 10 mM glucose, 10 mM HEPES, 10 mM BDM; pH 7.4)) for single parameter voltage
219 optical mapping. Slices were paced at 1 Hz frequency, 2 ms duration at an amplitude of 1.5X
220 the threshold for stimulation using a platinum bipolar pacing wire positioned at the center of the
221 slice. Slices were excited using excitation light at 520 ± 5 nm and the emitted light was collected
222 by a tandem lens optical mapping system, filtered using a 610 ± 20 nm filter and recorded using
223 the SciMedia Ultima L-type CMOS cameras.

224 Optical signals were analyzed as previously described[35, 36]. Briefly, activation times were
225 defined as the time of maximum first derivative of the fluorescence signal during the upstroke.
226 End of action potential and calcium transients were defined as the point where the signal returns
227 to 80% of its total signal amplitude. Conduction velocity was determined in the transverse
228 direction of propagation using activation times and known interpixel resolution.

229 **Cap analysis of gene expression:** For high-throughput analysis of transcriptional starting
230 point and identification of promoter usage, we performed cap analysis of gene expression
231 (CAGE). Total RNA from the cultured slices was extracted using the RNeasy Fibrous Tissue
232 Mini Kit according to the manufacture's protocol. Library preparation and sequencing with
233 HiSeq2500 was performed according to the Morioka *et al* protocol[37]. Read mapping was
234 performed with Burrows-Wheeler Aligner[38]; subsequent analysis of reads into decomposition
235 peak identification (DPI) and transcription start site-like peaks was performed with *DPI1*
236 (https://github.com/hkawaji/dpi1/) followed by *TomeTools TSSClassifier*
237 (https://sourceforge.net/projects/tometools/). Differential expression analysis was performed
238 with *edgeR*[39], gene ontology (GO) with *limma*[40], and heatmap plotting with *pheatmap*
239 (https://CRAN.R-project.org/package=pheatmap).

240

241 **Results**

242 **hiPSC-CMs demonstrate doxorubicin cardiotoxicity but not sunitinib**

243 A major distinction between the heart slice preparation and hiPSC-CMs is the retention of
244 multiple cell types in heart slices. It has been reported hiPSC-CMs is able to demonstrate the
245 cardiotoxic phenotype of doxorubicin in nanomolar concentrations but not for nanomolar
246 concentrations of sunitinib[30]. First we needed to reproduce these findings in our hands,
247 therefore, we tested different the effect of different concentrations of doxorubicin, and sunitinib
248 on hiPS-CMs viability using caspapse3/7 apoptosis assay over 48 hours. aspirin and erlotinib
249 (non-cardiotoxic TKI) used as negative controls (Figure 1). consistent with the previous report[30],
250 sunitinib did not show any cardiotoxicity in hiPSC-CMs at 500 nM or 1 μM concentrations as
251 assessed by caspase3/7 apoptosis assay (Figure 1d-f). Sunitinib at 60 μM showed acute
252 apoptotic response within one hour of addition, therefore, no more fluorescence was detected

253 over the course of the experiment using this concentration (Figure 1d-f). However, doxorubicin
254 as low as 500 nM demonstrated the expected cardiotoxicity on hiPSC-CMs and the negative
255 controls (aspirin and erlotinib (non-cardiotoxic TKI) did not show any cardiotoxic effect on
256 hiPSC-CMs up to 60 μM (Figure 1a-c).

257 **Effect of cardiotoxins on heart slices viability and cardiomyocyte integrity**

258 Pig heart slice exposure to these concentrations of cardiotoxins for 48 h resulted in a
259 significant decline in the general viability of the tissue as assessed by the MTT viability assay
260 (Figure 2a). Structurally, following the tissue exposure to doxorubicin, there was a decrease in
261 the gap junction protein, connexin-43, expression starting at the lowest concentration (Figure
262 1b). Heart slices treated with trastuzumab showed disruption in connexin-43 localization at the
263 gap junction accompanied by a lower level of troponin expression starting at the lowest
264 concentration (Figure 2b). Interestingly, low concentration sunitinib treatment did not appear to
265 have an effect on the structure of the tissue slices; however, the higher concentrations showed
266 disruption of connexin-43 localization (Figure 2b).

267 **Effect of cardiotoxins on heart slices calcium homeostasis**

268 We next tested the effects of cardiotoxins on the calcium homeostasis within the pig heart
269 slices after 48 h exposure. All high concentrations of cardiotoxins completely abolished the
270 calcium transients (Supp Movie 3, 4, 6, 7, 9 and 10) compared with the control (Supp movie 1),
271 However, as the lower concentrations are more clinically relevant, they demonstrated several of
272 the clinically-observed effects on the cardiac contractility and rhythm[5]. Treatment with 100 nM
273 doxorubicin showed abolished calcium transients, indicating direct cardiomyocyte damage
274 (Figure 3 Supp movie 2). Trastuzumab (1 μg) (Figure 3, Supp movie 5) or sunitinib (100 nM)
275 (Figure 3, Supp movie 8) treatment resulted in severe disruption in calcium homeostasis within
276 the heart slices.

277 **Mechanistic understanding of the cardiotoxic effects**

278 Transcriptomic analyses were performed to understand the mechanism behind the
279 responses of the pig heart slice to cardiotoxins. The top significant up/downregulated gene
280 ontology (GO) terms for tissue treated with 100 nM of doxorubicin are shown in Figure 4a-c. The
281 top downregulated GO terms were genes responsible for cardiac muscle and development as
282 well as cellular division genes. The top upregulated GO terms were genes involved in
283 oxidation/reduction and inflammatory response that is consistent with the known free radical
284 induction by doxorubicin. Figure 5a-c shows the up/downregulated genes in heart slices treated
285 with 1 μg trastuzumab for 48 h. The downregulated genes are mainly contractile genes, which
286 indicates a direct effect on the cardiomyocytes structure. Figure 6a-c shows the
287 up/downregulated GO terms in heart slices treated with 100 nM sunitinib. Sunitinib treatment
288 resulted in significant downregulation in angiogenesis-related genes.

289 **Human heart slices can reliably and consistently predict doxorubicin cardiotoxicity**

290 The experiments described above with viability, structure and calcium assays were
291 performed on pig hearts to ensure consistency between the tissues. However, the ultimate goal
292 of the field is to predict cardiotoxicity in human heart tissue, therefore, we used healthy human
293 heart tissue to demonstrate doxorubicin cardiotoxicity on functional and transcriptomics levels.
294 To ensure gender consistency between the human hearts in demonstrating the mechanism of
295 doxorubicin cardiotoxicity, we used 2 female and 4 male hearts. Consistent with the pig heart
296 data, electrophysiological remodeling was also observed in human heart slices. Significant
297 slowing of cardiac conduction velocity in the transverse direction of propagation in response to
298 50 μM doxorubicin exposure for 24 h was observed in all human hearts used within the
299 experiment[36] (Figure 7a-b). These results are consistent with reports of acute electrophysiologic
300 alterations in some patients treated with doxorubicin[41]. Furthermore, Cap analysis of gene
301 expression (CAGE) transcriptome analysis revealed 1433 differentially expressed genes in

302 control and 2172 differentially expressed genes at the promoter level in doxorubicin-treated
303 human cardiac slices as illustrated in (Figure 7c). GO analysis revealed that most differentially
304 expressed genes were associated with DNA repair, oxidation-reduction, mitochondria viability
305 and oxidative phosphorylation, which are likely to be related to the damage of the energetic
306 capacity of the cardiomyocytes (Figure 7d). Hierarchical clustering analysis further illustrated
307 different clustering of control and doxorubicin-treated human cardiac organotypic slices (Figure
308 7e). Importantly, these analyses show the consistency of the transcriptomic response to
309 doxorubicin among different human subjects (Figure 7e).

310 **Discussion**

311 Drug-induced cardiotoxicity is a major cause of drug attrition[42]. Therefore, there is a pressing
312 need for predictable preclinical screening strategies for cardiovascular toxicities associated with
313 emerging new drugs prior to clinical trials. The recent consideration of hiPSC-CMs for testing
314 drug toxicity provided a partial solution for some contexts of use but did not solve the overall
315 need in predicting effects in a diversity of functional cardiac modes of failure e.g., effects on
316 endothelial cells, microvasculature or smooth muscle cells[15, 16]. In addition to fetal-like
317 properties, a single cell type does not replicate the complexity of a 3D heart tissue that contains
318 multiple cell types and biological connections. For the first time, we were able to demonstrate
319 the clinical cardiotoxic phenotype of three mechanistically different cardiotoxic drugs using a 3D
320 pig heart slice culture model.

321 The first drug that we tested was an anthracycline, which is a class of antibiotics discovered
322 over 60 years ago and used to treat many different cancers[43]. Doxorubicin is one of the
323 commonly used anthracyclines for the treatment of lymphoma, leukemia, sarcoma, and breast
324 cancer[43]. The anticancer activity of doxorubicin results from DNA and RNA synthesis
325 disruption[43], attenuated DNA repair[44], and generation of free radicals which damage the DNA[45].
326 Even though doxorubicin is an effective and commonly used anticancer therapy, its use is

327 limited by its cardiotoxicity. Between 5% and 23% of the patients that receive doxorubicin
328 develop diminished exercise capacity and progressive heart failure symptoms[46, 47]. Toxicity
329 mechanisms of doxorubicin dependent on patient-specific properties are still poorly understood,
330 despite being a compound extensively studied for decades; doxorubicin has been found to
331 induce multiple forms of direct cellular injury to cardiomyocytes as a result of free radical
332 production induced by the quinone group[48]. This direct damage to cardiomyocytes has been
333 demonstrated in hiPSC-CMs[28, 30]. Consistent with these reports, our pig and human heart slice
334 models recapitulated the known response to doxorubicin, as our RNAseq data show
335 downregulation of genes responsible for cardiac development and cellular division and
336 upregulation of genes involved in oxidation/reduction and inflammatory response, which is
337 congruent with the known oxidative stress induced by doxorubicin[30].

338 The second cardiotoxin is a HER2-targeted agent (Trastuzumab) that targets and inhibit
339 HER2/*neu* receptors (also known as ERBB2). Here we used trastuzumab, the first approved
340 HER2-targeted agent[49]. Trastuzumab is a humanized monoclonal antibody that exerts its
341 anticancer effect through blocking the activation of the HER2(ERBB2)/*neu* receptor, leading to
342 the inhibition of epidermal growth factors/HER2 ligand receptor activity and disrupting the
343 phosphorylation of tyrosine kinases which are critical regulators of the cell cycle[49]. It has been
344 noted that trastuzumab treatment results in asymptomatic cardiac dysfunction and, less often,
345 symptomatic heart failure in some patients[50]. Trastuzumab-induced cardiotoxicity is thought to
346 be driven by disruption of ERBB2/neuregulin signaling in cardiomyocytes, which is critical for
347 normal myocyte growth, survival, and homeostasis[51]. The trastuzumab-induced direct
348 cardiomyocyte damage phenotype and mechanism has been recently modeled in hiPSC-CMs[29,
349 52]. Consistent with these findings, pig heart slices treated with trastuzumab showed direct
350 cardiomyocyte damage, as evidenced by disruption of calcium homeostasis and downregulation
351 of cardiac contractile gene expression.

352 Sunitinib was the third cardiotoxin tested, a tyrosine kinase and angiogenesis inhibitors
353 (TKIs), which directly inhibits angiogenesis through inhibition of vascular endothelial growth
354 factor (VEGF). This is usually accompanied by cardiovascular toxicity related to increased blood
355 pressure[53]. Other direct cardiac toxicities included cardiac systolic dysfunction, which has been
356 observed in patients treated with sunitinib and sorafenib[54] and has been attributed to the
357 disruption of the coronary microvascular pericytes leading to hypoxia of cardiomyocytes[55] and
358 cardiomyopathy. It was not possible to model these indirect effects using hiPSC-CMs, as
359 nanomolar concentrations of sunitinib treatment have no obvious cardiotoxic effects on hiPSC-
360 CMs due to its indirect effect on cardiomyocytes as indicated by our own data (Figure 1) and
361 others[30]. However, in our heart slice system we were able to demonstrate clearly that although
362 sunitinib (as low as 100nM) causes no major damage to the cardiomyocyte structure, it induces
363 disruption of the angiogenic gene program in the heart tissue, which is consistent with its clinical
364 effects.

365 In conclusion, the results of this study suggest that the heart slice culture system is a
366 promising platform for modeling cardiotoxicity phenotypes and mechanisms. These data
367 suggest that this system will be useful to test acute and subacute cardiotoxicity of new
368 therapeutics.

369

370 **References**

371 1. Mladenka P, Applova L, Patocka J, Costa VM, Remiao F, Pourova J, Mladenka A,
372 Karlickova J, Jahodar L, Voprsalova M, Varner KJ, Sterba M, Tox OER, Researchers CHK and
373 Collaborators. Comprehensive review of cardiovascular toxicity of drugs and related agents.
374 *Med Res Rev*. 2018;38:1332-1403.

375 2. Kocadal K, Saygi S, Alkas FB and Sardas S. Drug-associated cardiovascular risks: A
376 retrospective evaluation of withdrawn drugs. *North Clin Istanb*. 2019;6:196-202.
377 3. Mercuro G, Cadeddu C, Piras A, Dessi M, Madeddu C, Deidda M, Serpe R, Massa E
378 and Mantovani G. Early epirubicin-induced myocardial dysfunction revealed by serial tissue
379 Doppler echocardiography: correlation with inflammatory and oxidative stress markers. *The*
380 *oncologist*. 2007;12:1124-33.
381 4. Lenneman CG and Sawyer DB. Cardio-Oncology: An Update on Cardiotoxicity of
382 Cancer-Related Treatment. *Circulation Research*. 2016;118:1008-20.
383 5. Moslehi JJ. Cardiovascular Toxic Effects of Targeted Cancer Therapies. *The New*
384 *England journal of medicine*. 2016;375:1457-1467.
385 6. Yang B and Papoian T. Preclinical approaches to assess potential kinase inhibitor-
386 induced cardiac toxicity: Past, present and future. *J Appl Toxicol*. 2018;38:790-800.
387 7. Knudsen ES and Witkiewicz AK. The Strange Case of CDK4/6 Inhibitors: Mechanisms,
388 Resistance, and Combination Strategies. *Trends Cancer*. 2017;3:39-55.
389 8. Han X, Zhou Y and Liu W. Precision cardio-oncology: understanding the cardiotoxicity of
390 cancer therapy. *NPJ precision oncology*. 2017;1:31.
391 9. Hughes JP, Rees S, Kalindjian SB and Philpott KL. Principles of early drug discovery.
392 *British journal of pharmacology*. 2011;162:1239-49.
393 10. Van Norman GA. Limitations of Animal Studies for Predicting Toxicity in Clinical Trials: Is
394 it Time to Rethink Our Current Approach? *Journal of the American College of Cardiology: Basic*
395 *to Translational Science*. 2019;4:845-854.
396 11. Van Norman GA. Limitations of Animal Studies for Predicting Toxicity in Clinical Trials:
397 Part 2: Potential Alternatives to the Use of Animals in Preclinical Trials. *Journal of the American*
398 *College of Cardiology: Basic to Translational Science*. 2020;5:387-397.
399 12. Hearse DJ and Sutherland FJ. Experimental models for the study of cardiovascular
400 function and disease. *Pharmacological research*. 2000;41:597-603.

401 13. Houser SR, Margulies KB, Murphy AM, Spinale FG, Francis GS, Prabhu SD, Rockman
402 HA, Kass DA, Molkentin JD, Sussman MA and Koch WJ. Animal Models of Heart Failure.
403 *Circulation Research*. 2012;111:131-150.
404 14. Clark M and Steger-Hartmann T. A big data approach to the concordance of the toxicity
405 of pharmaceuticals in animals and humans. *Regul Toxicol Pharmacol*. 2018;96:94-105.
406 15. Gintant G, Burridge P, Gepstein L, Harding S, Herron T, Hong C, Jalife J and Wu JC.
407 Use of Human Induced Pluripotent Stem Cell-Derived Cardiomyocytes in Preclinical Cancer
408 Drug Cardiotoxicity Testing: A Scientific Statement From the American Heart Association.
409 *Circulation Research*. 2019;125:e75-e92.
410 16. Pang L, Sager P, Yang X, Shi H, Sannajust F, Brock M, Wu JC, Abi-Gerges N, Lyn-
411 Cook B, Berridge BR and Stockbridge N. Workshop Report: FDA Workshop on Improving
412 Cardiotoxicity Assessment With Human-Relevant Platforms. *Circulation Research*.
413 2019;125:855-867.
414 17. Ronaldson-Bouchard K, Ma SP, Yeager K, Chen T, Song L, Sirabella D, Morikawa K,
415 Teles D, Yazawa M and Vunjak-Novakovic G. Advanced maturation of human cardiac tissue
416 grown from pluripotent stem cells. *Nature*. 2018;556:239-243.
417 18. Bird SD, Doevendans PA, van Rooijen MA, Brutel de la Riviere A, Hassink RJ, Passier
418 R and Mummery CL. The human adult cardiomyocyte phenotype. *Cardiovascular Research*.
419 2003;58:423-434.
420 19. Pinto AR, Ilinykh A, Ivey MJ, Kuwabara JT, D'Antoni ML, Debuque R, Chandran A,
421 Wang L, Arora K, Rosenthal NA and Tallquist MD. Revisiting Cardiac Cellular Composition.
422 *Circulation Research*. 2016;118:400-9.
423 20. Kanisicak O, Khalil H, Ivey MJ, Karch J, Maliken BD, Correll RN, Brody MJ, SC JL,
424 Aronow BJ, Tallquist MD and Molkentin JD. Genetic lineage tracing defines myofibroblast origin
425 and function in the injured heart. *Nature Communications*. 2016;7:12260.

426 21. Fu X, Khalil H, Kanisicak O, Boyer JG, Vagnozzi RJ, Maliken BD, Sargent MA, Prasad
427 V, Valiente-Alandi I, Blaxall BC and Molkentin JD. Specialized fibroblast differentiated states
428 underlie scar formation in the infarcted mouse heart. *Journal of Clinical Investigations*.
429 2018;128:2127-2143.
430 22. Kretzschmar K, Post Y, Bannier-Helaouet M, Mattiotti A, Drost J, Basak O, Li VSW, van
431 den Born M, Gunst QD, Versteeg D, Kooijman L, van der Elst S, van Es JH, van Rooij E, van
432 den Hoff MJB and Clevers H. Profiling proliferative cells and their progeny in damaged murine
433 hearts. *Proceedings of the National Academy of Sciences of the United States of America*.
434 2018;115:E12245-E12254.
435 23. Glukhov AV, Fedorov VV, Kalish PW, Ravikumar VK, Lou Q, Janks D, Schuessler RB,
436 Moazami N and Efimov IR. Conduction Remodeling in Human End-Stage Nonischemic Left
437 Ventricular Cardiomyopathy. *Circulation*. 2012;125:1835-1847.
438 24. Lou Q, Fedorov VV, Glukhov AV, Moazami N, Fast VG and Efimov IR. Transmural
439 Heterogeneity and Remodeling of Ventricular Excitation-Contraction Coupling in Human Heart
440 Failure. *Circulation*. 2011;123:1881-1890.
441 25. Kang C, Qiao Y, Li G, Baechle K, Camelliti P, Rentschler S and Efimov IR. Human
442 Organotypic Cultured Cardiac Slices: New Platform For High Throughput Preclinical Human
443 Trials. *Scientific Reports*. 2016;6:28798.
444 26. Camelliti P, Al-Saud SA, Smolenski RT, Al-Ayoubi S, Bussek A, Wettwer E, Banner NR,
445 Bowles CT, Yacoub MH and Terracciano CM. Adult human heart slices are a multicellular
446 system suitable for electrophysiological and pharmacological studies. *Journal of molecular and*
447 *cellular cardiology*. 2011;51:390-398.
448 27. Ou Q, Jacobson Z, Abouleisa RRE, Tang XL, Hindi SM, Kumar A, Ivey KN, Giridharan
449 G, El-Baz A, Brittian K, Rood B, Lin YH, Watson SA, Perbellini F, McKinsey TA, Hill BG, Jones
450 SP, Terracciano CM, Bolli R and Mohamed TMA. Physiological Biomimetic Culture System for
451 Pig and Human Heart Slices. *Circulation Research*. 2019;125:628-642.

452 28. Burridge PW, Li YF, Matsa E, Wu H, Ong SG, Sharma A, Holmstrom A, Chang AC,
453 Coronado MJ, Ebert AD, Knowles JW, Telli ML, Witteles RM, Blau HM, Bernstein D, Altman RB
454 and Wu JC. Human induced pluripotent stem cell-derived cardiomyocytes recapitulate the
455 predilection of breast cancer patients to doxorubicin-induced cardiotoxicity. *Nat Med*.
456 2016;22:547-56.
457 29. Kitani T, Ong SG, Lam CK, Rhee JW, Zhang JZ, Oikonomopoulos A, Ma N, Tian L, Lee
458 J, Telli ML, Witteles RM, Sharma A, Sayed N and Wu JC. Human-Induced Pluripotent Stem Cell
459 Model of Trastuzumab-Induced Cardiac Dysfunction in Patients With Breast Cancer. *Circulation*.
460 2019;139:2451-2465.
461 30. Zhao L and Zhang B. Doxorubicin induces cardiotoxicity through upregulation of death
462 receptors mediated apoptosis in cardiomyocytes. *Scientific Reports*. 2017;7:44735.
463 31. Barpe DR, Rosa DD and Froehlich PE. Pharmacokinetic evaluation of doxorubicin
464 plasma levels in normal and overweight patients with breast cancer and simulation of dose
465 adjustment by different indexes of body mass. *Eur J Pharm Sci*. 2010;41:458-63.
466 32. Stemmler HJ, Schmitt M, Willems A, Bernhard H, Harbeck N and Heinemann V. Ratio of
467 trastuzumab levels in serum and cerebrospinal fluid is altered in HER2-positive breast cancer
468 patients with brain metastases and impairment of blood-brain barrier. *Anticancer Drugs*.
469 2007;18:23-8.
470 33. Takasaki S, Kawasaki Y, Kikuchi M, Tanaka M, Suzuka M, Noda A, Sato Y, Yamashita
471 S, Mitsuzuka K, Saito H, Ito A, Yamaguchi H, Arai Y and Mano N. Relationships between
472 sunitinib plasma concentration and clinical outcomes in Japanese patients with metastatic renal
473 cell carcinoma. *Int J Clin Oncol*. 2018;23:936-943.
474 34. Ou Q, Abouleisa RRE, Tang XL, Juhardeen HR, Meki MH, Miller JM, Giridharan G, El-
475 Baz A, Bolli R and Mohamed TMA. Slicing and Culturing Pig Hearts under Physiological
476 Conditions. *J Vis Exp*. 2020.

477 35. Kang C, Qiao Y, Li G, Baechle K, Camelliti P, Rentschler S and Efimov IR. Human
478 Organotypic Cultured Cardiac Slices: New Platform For High Throughput Preclinical Human
479 Trials. *Scientific Reports*. 2016;6:28798.
480 36. George SA, Brennan JA and Efimov IR. Preclinical Cardiac Electrophysiological
481 Assessment by Dual Voltage and Calcium Optical Mapping of Human Organotypic Cardiac
482 Slices. *J Vis Exp*. In Press.
483 37. Morioka MS, Kawaji H, Nishiyori-Sueki H, Murata M, Kojima-Ishiyama M, Carninci P and
484 Itoh M. Cap Analysis of Gene Expression (CAGE): A Quantitative and Genome-Wide Assay of
485 Transcription Start Sites. *Methods in molecular biology (Clifton, NJ*. 2020;2120:277-301.
486 38. Li H and Durbin R. Fast and accurate long-read alignment with Burrows-Wheeler
487 transform. *Bioinformatics (Oxford, England)*. 2010;26:589-95.
488 39. McCarthy DJ, Chen Y and Smyth GK. Differential expression analysis of multifactor
489 RNA-Seq experiments with respect to biological variation. *Nucleic Acids Res*. 2012;40:4288-97.
490 40. Ritchie ME, Phipson B, Wu D, Hu Y, Law CW, Shi W and Smyth GK. limma powers
491 differential expression analyses for RNA-sequencing and microarray studies. *Nucleic Acids Res*.
492 2015;43:e47.
493 41. Cai F, Luis MAF, Lin X, Wang M, Cai L, Cen C and Biskup E. Anthracycline-induced
494 cardiotoxicity in the chemotherapy treatment of breast cancer: Preventive strategies and
495 treatment. *Mol Clin Oncol*. 2019;11:15-23.
496 42. Onakpoya IJ, Heneghan CJ and Aronson JK. Post-marketing withdrawal of 462
497 medicinal products because of adverse drug reactions: a systematic review of the world
498 literature. *BioMed Central Medicine*. 2016;14:10.
499 43. Geisberg CA and Sawyer DB. Mechanisms of anthracycline cardiotoxicity and strategies
500 to decrease cardiac damage. *Curr Hypertens Rep*. 2010;12:404-10.
501 44. Pang B, Qiao X, Janssen L, Velds A, Groothuis T, Kerkhoven R, Nieuwland M, Ovaa H,
502 Rottenberg S, van Tellingen O, Janssen J, Huijgens P, Zwart W and Neefjes J. Drug-induced

503 histone eviction from open chromatin contributes to the chemotherapeutic effects of doxorubicin.
504 *Nature Communications*. 2013;4:1908.
505 45. Zhang S, Liu X, Bawa-Khalfe T, Lu LS, Lyu YL, Liu LF and Yeh ET. Identification of the
506 molecular basis of doxorubicin-induced cardiotoxicity. *Nat Med*. 2012;18:1639-42.
507 46. Steinherz LJ, Steinherz PG, Tan CT, Heller G and Murphy ML. Cardiac toxicity 4 to 20
508 years after completing anthracycline therapy. *JAMA*. 1991;266:1672-7.
509 47. Cardinale D, Colombo A, Lamantia G, Colombo N, Civelli M, De Giacomi G, Rubino M,
510 Veglia F, Fiorentini C and Cipolla CM. Anthracycline-induced cardiomyopathy: clinical relevance
511 and response to pharmacologic therapy. *J Am Coll Cardiol*. 2010;55:213-20.
512 48. Horenstein MS, Vander Heide RS and L'Ecuyer TJ. Molecular basis of anthracycline-
513 induced cardiotoxicity and its prevention. *Mol Genet Metab*. 2000;71:436-44.
514 49. Slamon DJ, Leyland-Jones B, Shak S, Fuchs H, Paton V, Bajamonde A, Fleming T,
515 Eiermann W, Wolter J, Pegram M, Baselga J and Norton L. Use of chemotherapy plus a
516 monoclonal antibody against HER2 for metastatic breast cancer that overexpresses HER2. *The*
517 *New England journal of medicine*. 2001;344:783-92.
518 50. Onitilo AA, Engel JM and Stankowski RV. Cardiovascular toxicity associated with
519 adjuvant trastuzumab therapy: prevalence, patient characteristics, and risk factors. *Ther Adv*
520 *Drug Saf*. 2014;5:154-66.
521 51. Crone SA, Zhao YY, Fan L, Gu Y, Minamisawa S, Liu Y, Peterson KL, Chen J, Kahn R,
522 Condorelli G, Ross J, Jr., Chien KR and Lee KF. ErbB2 is essential in the prevention of dilated
523 cardiomyopathy. *Nat Med*. 2002;8:459-65.
524 52. Kurokawa YK, Shang MR, Yin RT and George SC. Modeling trastuzumab-related
525 cardiotoxicity in vitro using human stem cell-derived cardiomyocytes. *Toxicol Lett*. 2018;285:74-
526 80.

527 53. Pouessel D and Culine S. High frequency of intracerebral hemorrhage in metastatic
528 renal carcinoma patients with brain metastases treated with tyrosine kinase inhibitors targeting
529 the vascular endothelial growth factor receptor. *Eur Urol*. 2008;53:376-81.
530 54. Uraizee I, Cheng S and Moslehi J. Reversible cardiomyopathy associated with sunitinib
531 and sorafenib. *The New England journal of medicine*. 2011;365:1649-50.
532 55. Chintalgattu V, Rees ML, Culver JC, Goel A, Jiffar T, Zhang J, Dunner K, Jr., Pati S,
533 Bankson JA, Pasqualini R, Arap W, Bryan NS, Taegtmeyer H, Langley RR, Yao H, Kupferman
534 ME, Entman ML, Dickinson ME and Khakoo AY. Coronary microvascular pericytes are the
535 cellular target of sunitinib malate-induced cardiotoxicity. *Sci Transl Med*. 2013;5:187ra69.

536

Acknowledgments

TMAM is supported by NIH grants R01HL147921 and P30GM127607 and American Heart Association grant 16SDG29950012. The authors also acknowledge NIH grants P30GM127607 (BGH), R01HL130174 (BGH), R01HL147844 (BGH), R01ES028268 (BGH), GM127607 (DJC), P01HL78825 (RB, BGH) and UM1HL113530 (RB), Leducq Foundation RHYTHM grant (IRE), R01HL126802 (IRE), R44HL139248 (IRE) and an American Heart Association Postdoctoral fellowship (19POST34370122) to SAG. We acknowledge the guidance of Ruslan Deviatiiarov from the Institute of Fundamental Medicine and Biology. Kazan Federal University, Russia in the Cap Analysis of Gene expression data analysis.

Author contributions

J.M.M, M.H.M, Q.O, S.A.G.: collection and analysis of data, manuscript writing, and final approval of manuscript; A.G., R.R.E.A., X-L.T., B.M.A. collection and analysis of data; G.A.G., A.E., B.G.H., J.S., D.J.C., J.M., R.B., A.J.S.R, I.R.E, and T.M.A.M: conception and design, manuscript writing, and final approval of manuscript.

Competing Interests

TMAM, holds equities in Tenaya Therapeutics. GAG, is consultant for NuPulseCV. The other authors report no conflicts.

Disclaimer

This article reflects the views of the authors and should not be construed to represent the views or policies of the FDA

559 **Figure legends**

560 **Figure 1. Pro-apoptotic effect of doxorubicin and sunitinib on hiPSC-CMs:** Kinetics of
561 caspase-3/7 activation in hiPSC-CMs exposed to a range of concentrations of **(a)** aspirin (non-
562 toxic drug), **(b)** doxorubicin (cardiotoxin), **(c)** erlotinib (non-cardiotoxic TKI) and **(d)** sunitinib
563 (cardiotoxic TKI) over 48 h. DMSO in the medium at a concentration of 0.1% (v/v) was used as
564 a control. (A-D) Variations in total caspase integrated intensity was calculated from fluorescent
565 images of the caspase-3/7 green dye acquired every hour, which captured the extent of
566 apoptosis within cultured cells. Acute apoptotic effects were detected upon exposing cells to 60
567 μM of sunitinib as noted by the arrow in **(d)**. **(e and f)** Phase microscopy images of cells
568 acquired when 60 μM of sunitinib was added to cells **(e)** and one hour after being exposure **(f)**,
569 where total cell detachment was observed. Scale bar: 200 μm.

570 **Figure 2. Effect of cardiotoxins on heart slice viability and structure: (a)** Bar graph shows
571 the quantification of heart slice viability after 2 days of treatment with the corresponding
572 cardiotoxin using MTT assay (n=2 independent experiments, 4 replicates in each, One-Way
573 ANOVA test was conducted to compare between groups; *P<0.05 compared to the control). **(b)**
574 Representative immunofluorescence images showing the expression of connexin 43 (red) in
575 cardiomyocytes (green) in cross sections taken from heart tissue slices treated for 2 days with
576 the corresponding concentration of the cardiotoxin (Scale bar, 100 μm). These representative
577 images have been reproducible over 2 independent experiments with 3 technical replicates in
578 each experiment; however, the lack of reliable tools for quantifying localization of connexin 43
579 has limited our ability for quantification.

580 **Figure 3. Effect of cardiotoxins on heart slices functionality and calcium homeostasis: (a)**
581 Representative calcium traces from day 2 cultured control slices and heart slices treated with
582 the corresponding concentration of each cardiotoxin for 2 days. Transients were recorded after
583 loading the heart slices with Fluo-4 calcium dye and using 1 Hz/20 V electrical stimulation at the

584 time of recording. **(b)** Scoring of calcium transient amplitude as indication of the cardiomyocyte
585 function from slices treated with each cardiotoxin (n=36 cells in each group from 2 independent
586 experiments).

587 **Figure 4. Differential gene expression in slices treated with 100 nM doxorubicin: (a)**
588 Volcano plot showing significant changes in gene expression in 100nM doxorubicin (Dox)
589 treated tissue. Bar graph shows the GO terms for the significantly downregulated **(b)** or
590 upregulated **(C)** genes from RNA-seq data between control heart slices and heart slices treated
591 with 100nM doxorubicin (n=2 pig hearts).

592 **Figure 5. Differential gene expression in slices treated with 1µg trastuzumab: (a)** Volcano
593 plot demonstrating the genes which are significantly different between control heart slice and
594 slices treated with 1µg trastuzumab. Bar graph shows the GO terms for the significantly
595 downregulated **(b)** or upregulated **(c)** genes from RNA-seq data between control heart slices
596 and heart slices treated with 1µg trastuzumab (n=2 pig hearts).

597 **Figure 6. Differential gene expression in slices treated with 100nM sunitinib: (a)** Volcano
598 plot demonstrating the genes which are significantly different between control heart slice and
599 slices treated with 100nM sunitinib. Bar graph shows the GO terms for the significantly
600 downregulated **(b)** or upregulated **(c)** genes from RNA-seq data between control heart slices
601 and heart slices treated with 100nM sunitinib (n=2 pig hearts).

602 **Figure 7. Doxorubicin toxicity in human heart slices**: **(a)** Activation maps obtained by optical
603 mapping of human cardiac organotypic slices cultured for ~24 h with or without doxorubicin (50
604 µM). Crowding of activation lines in the transverse direction indicate conduction slowing with
605 doxorubicin treatment. **(b)** Average transverse conduction velocity determined from human
606 cardiac slices with and without doxorubicin treatment. Transverse conduction velocity was
607 significantly slower in doxorubicin treated slices (n=7, $p<0.05$). **(c)** Differentially expressed

608 genes between control and doxorubicin-treated human cardiac organotypic slices following Cap
609 Analysis of Gene Expression (n=3). **(d)** Gene ontology (GO) enrichment analysis of differentially
610 expressed genes in control and doxorubicin-treated slices. BP: biological process, CC: cellular
611 component, MF: molecular function (n=3). **(e)** Heat map demonstrating hierarchical clustering of
612 differentially expressed genes (n=3). F: female, M: male.

613

Figure 1

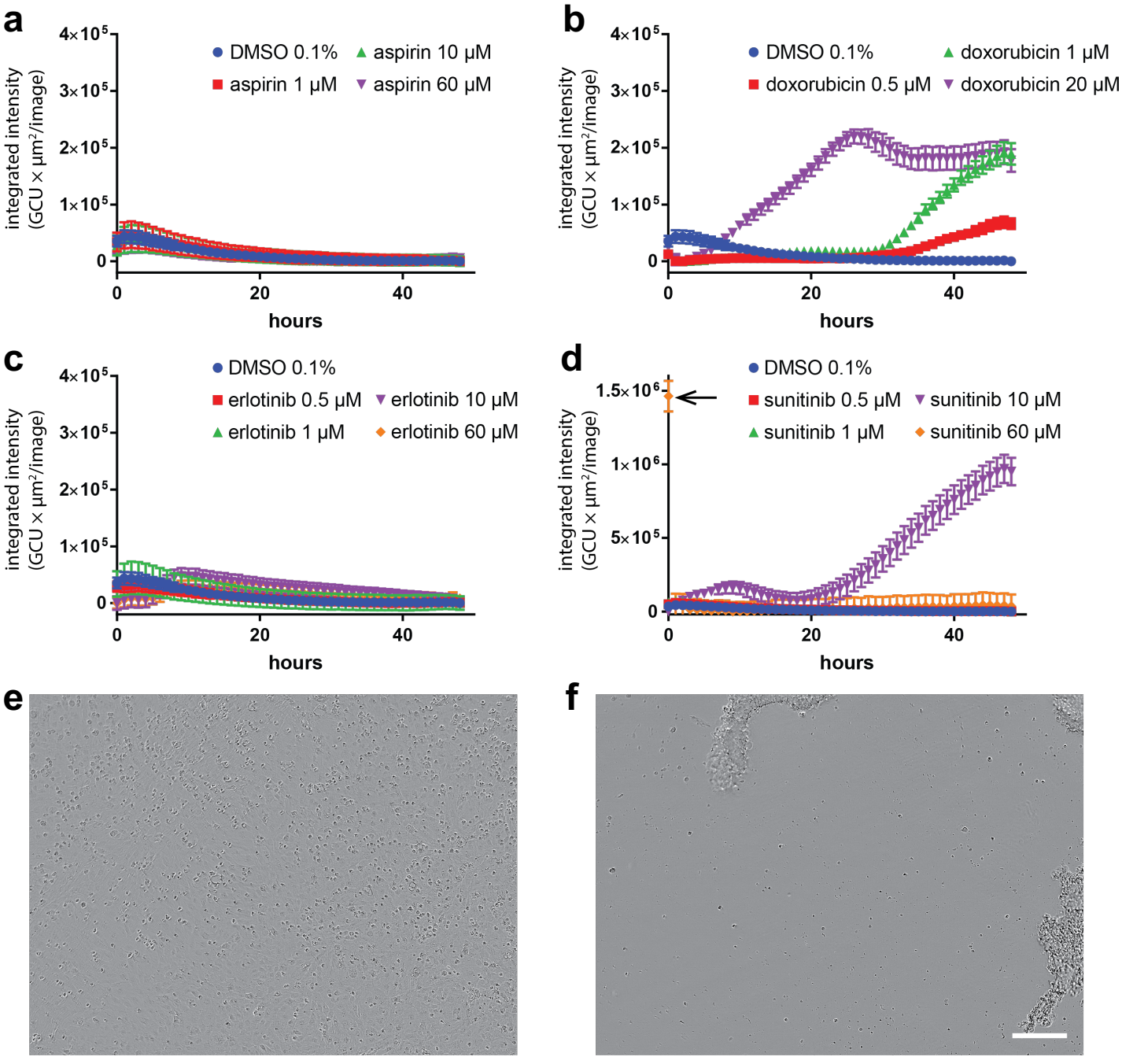
a
DMSO 0.1%
aspirin 1 μM
aspirin 10 μM
aspirin 60 μM
integrated intensity (GCU × μm²/image)
4×10⁵
3×10⁵
2×10⁵
1×10⁵
0
0
20
40
hours
b
DMSO 0.1%
doxorubicin 0.5 μM
doxorubicin 1 μM
doxorubicin 20 μM
integrated intensity (GCU × μm²/image)
4×10⁵
3×10⁵
2×10⁵
1×10⁵
0
0
20
40
hours
c
DMSO 0.1%
erlotinib 0.5 μM
erlotinib 1 μM
erlotinib 10 μM
erlotinib 60 μM
integrated intensity (GCU × μm²/image)
4×10⁵
3×10⁵
2×10⁵
1×10⁵
0
0
20
40
hours
d
DMSO 0.1%
sunitinib 0.5 μM
sunitinib 1 μM
sunitinib 10 μM
sunitinib 60 μM
integrated intensity (GCU × μm²/image)
1.5×10⁶
1×10⁶
5×10⁵
0
0
20
40
hours
e
f

Figure 2

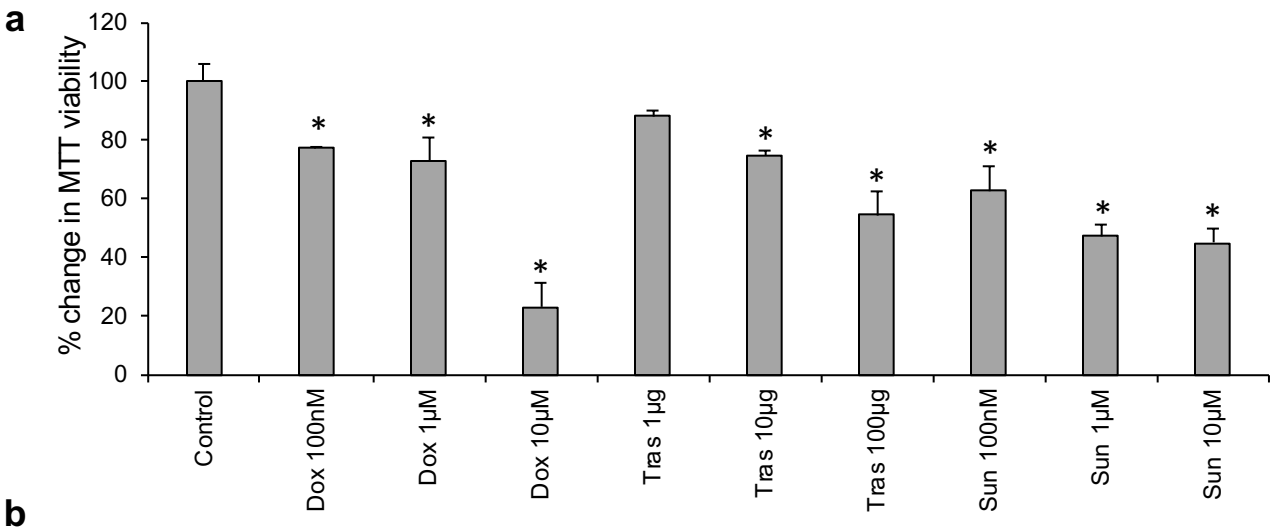
a
% change in MTT viability
120
100
80
60
40
20
0
Control
Dox 100nM
Dox 1μM
Dox 10μM
Tras 1μg
Tras 10μg
Tras 100μg
Sun 100nM
Sun 1μM
Sun 10μM

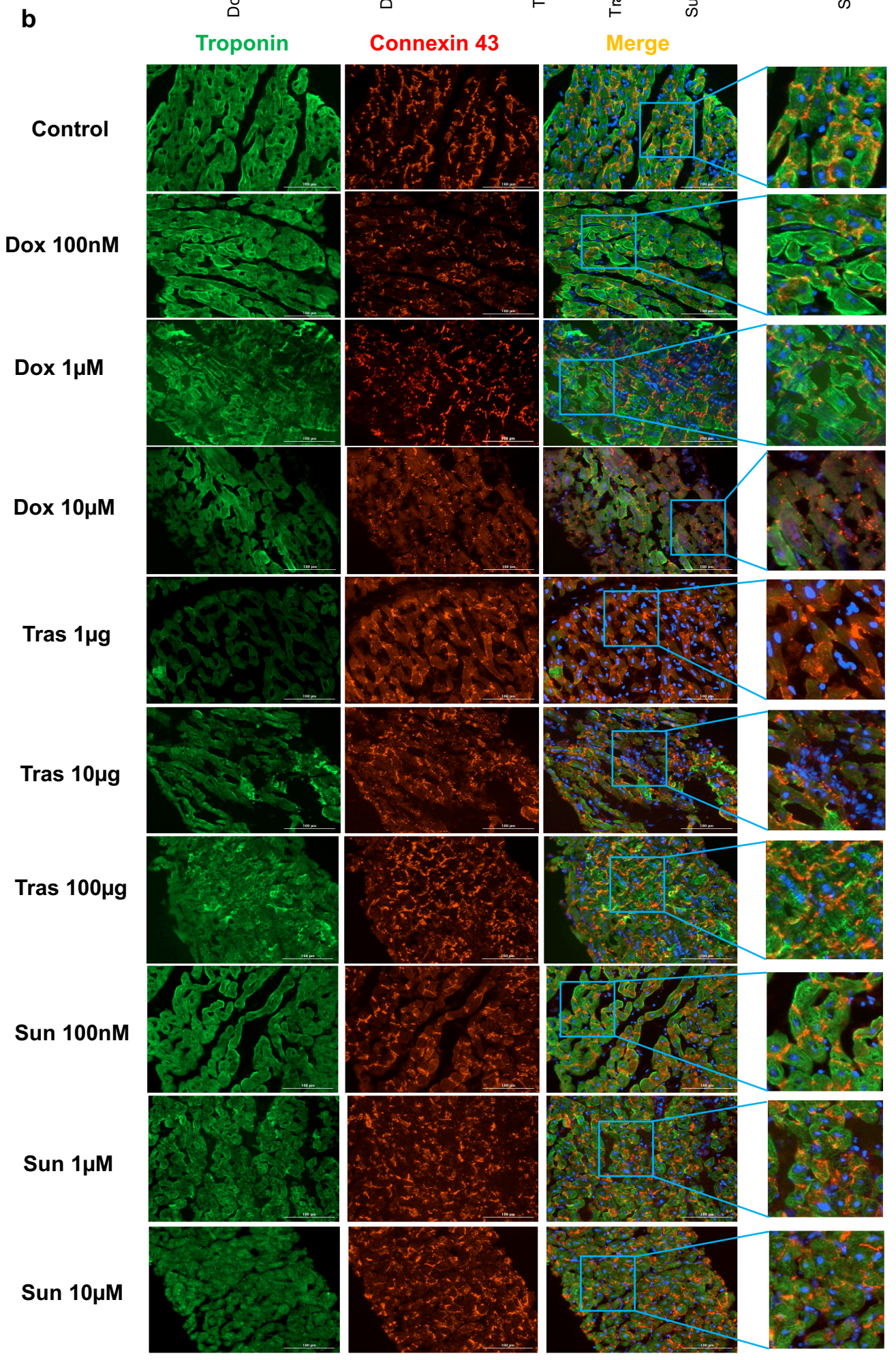
b
Troponin
Connexin 43
Merge
Control
Dox 100nM
Dox 1μM
Dox 10μM
Tras 1μg
Tras 10μg
Tras 100μg
Sun 100nM
Sun 1μM
Sun 10μM

Figure 3

a

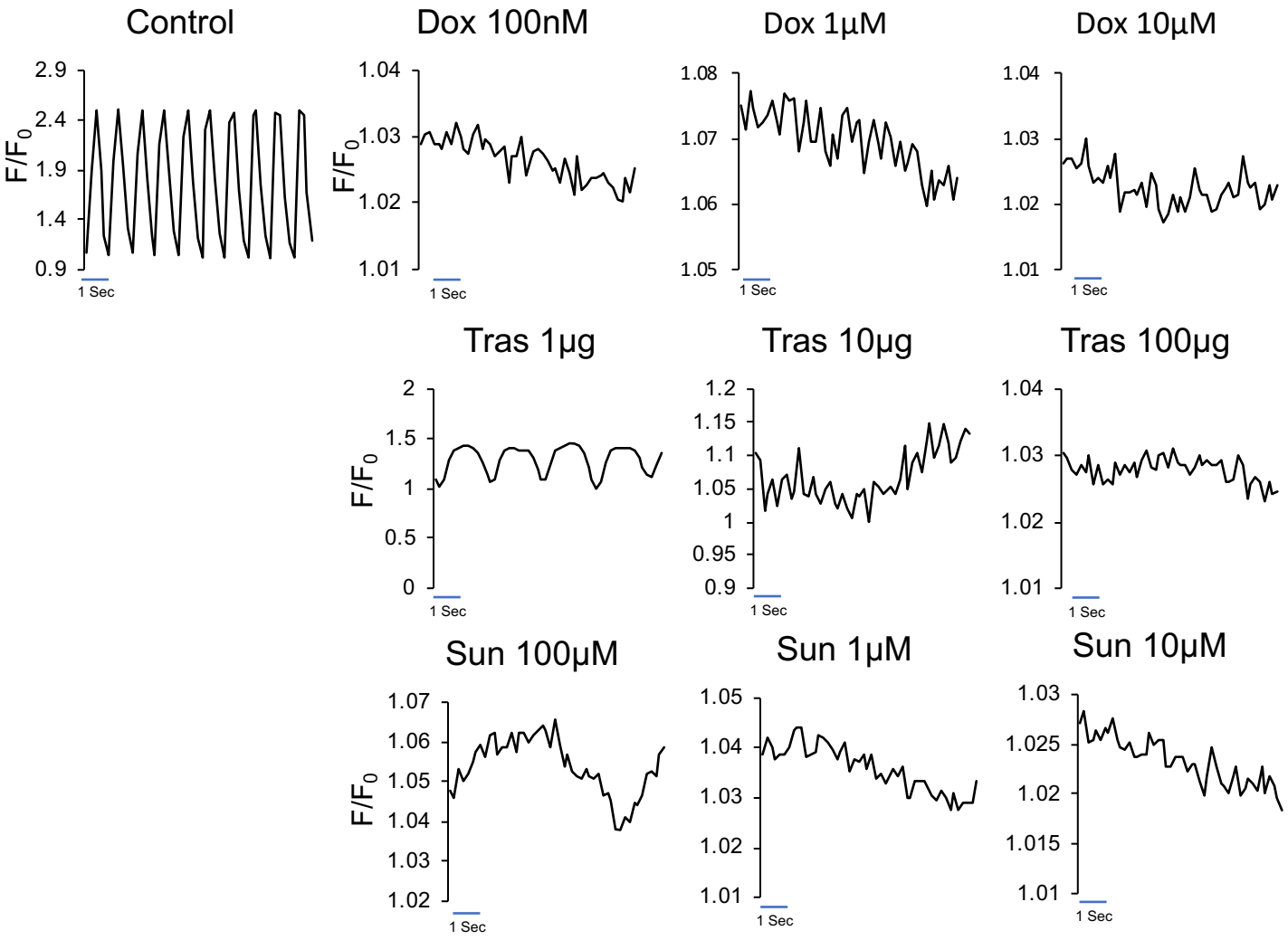

b

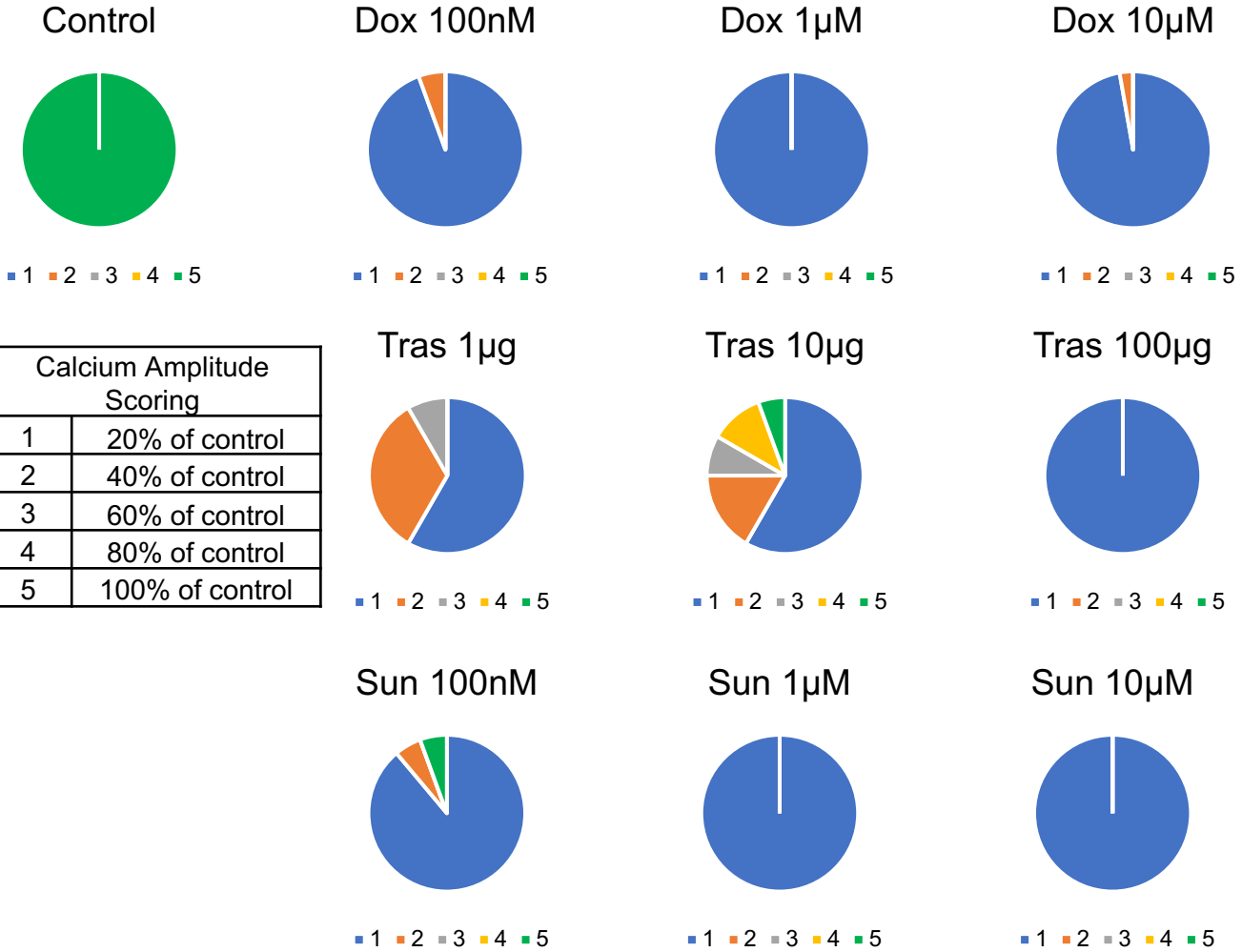

Calcium Amplitude Scoring	
1	20% of control
2	40% of control
3	60% of control
4	80% of control
5	100% of control

Figure 4

a

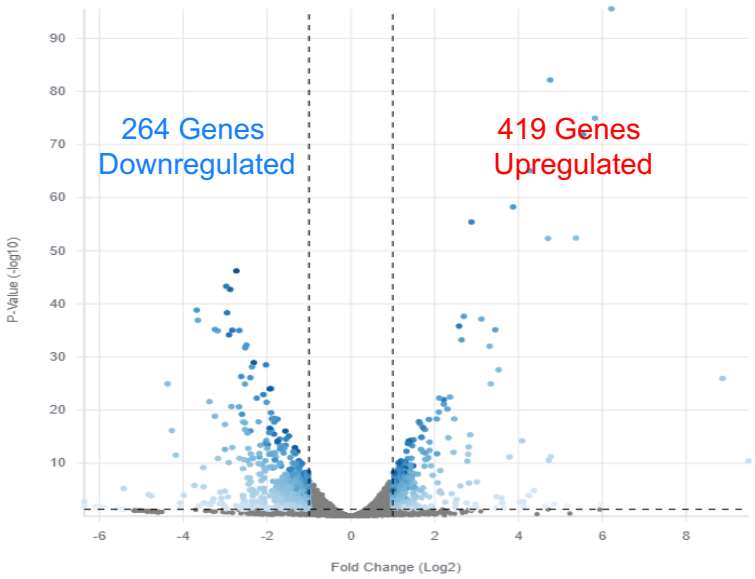
264 Genes
Downregulated
419 Genes
Upregulated
P-Value (-log10)
Fold Change (Log2)

b

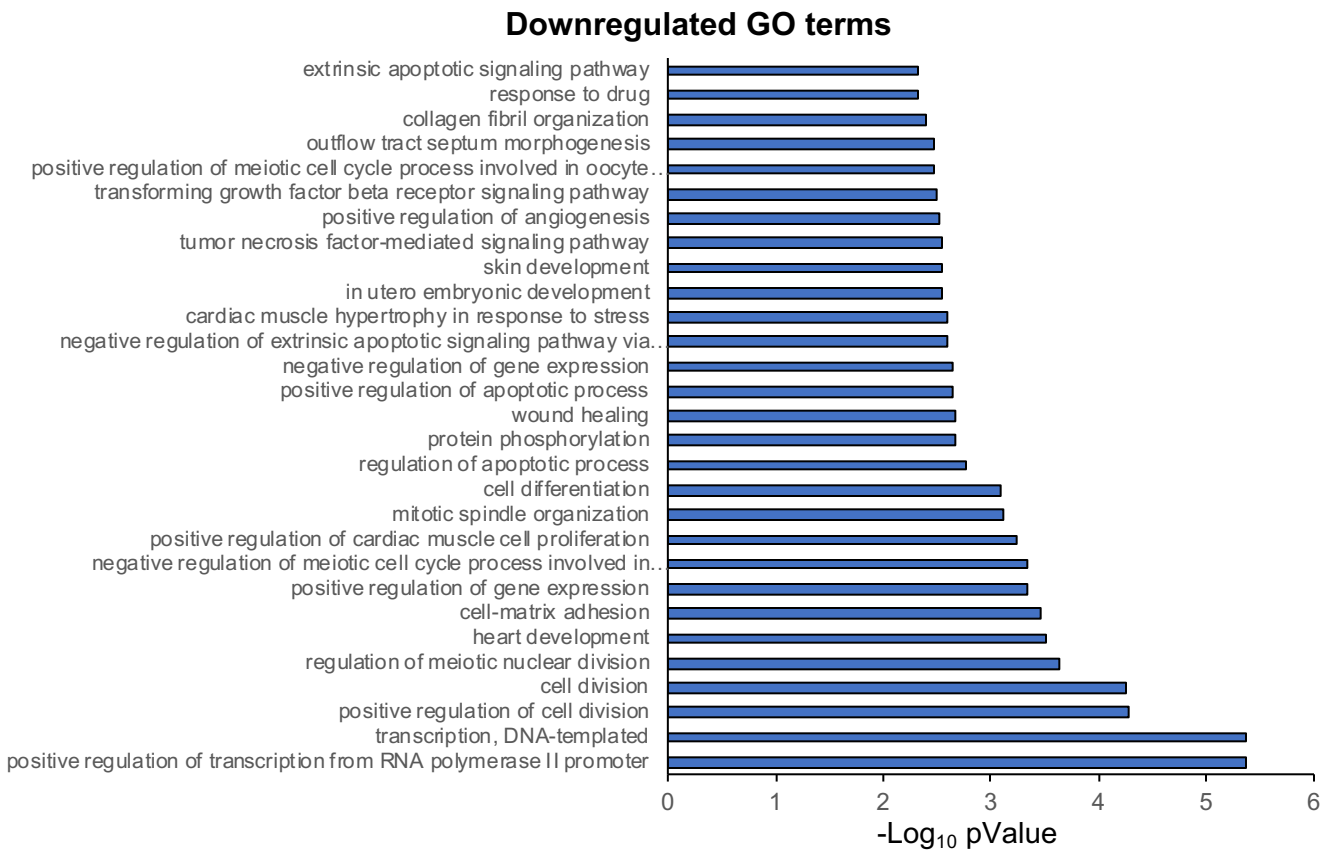
Downregulated GO terms
extrinsic apoptotic signaling pathway
response to drug
collagen fibril organization
outflow tract septum morphogenesis
positive regulation of meiotic cell cycle process involved in oocyte..
transforming growth factor beta receptor signaling pathway
positive regulation of angiogenesis
tumor necrosis factor-mediated signaling pathway
skin development
in utero embryonic development
cardiac muscle hypertrophy in response to stress
negative regulation of extrinsic apoptotic signaling pathway via..
negative regulation of gene expression
positive regulation of apoptotic process
wound healing
protein phosphorylation
regulation of apoptotic process
cell differentiation
mitotic spindle organization
positive regulation of cardiac muscle cell proliferation
negative regulation of meiotic cell cycle process involved in..
positive regulation of gene expression
cell-matrix adhesion
heart development
regulation of meiotic nuclear division
cell division
positive regulation of cell division
transcription, DNA-templated
positive regulation of transcription from RNA polymerase II promoter
-Log10 pValue

c

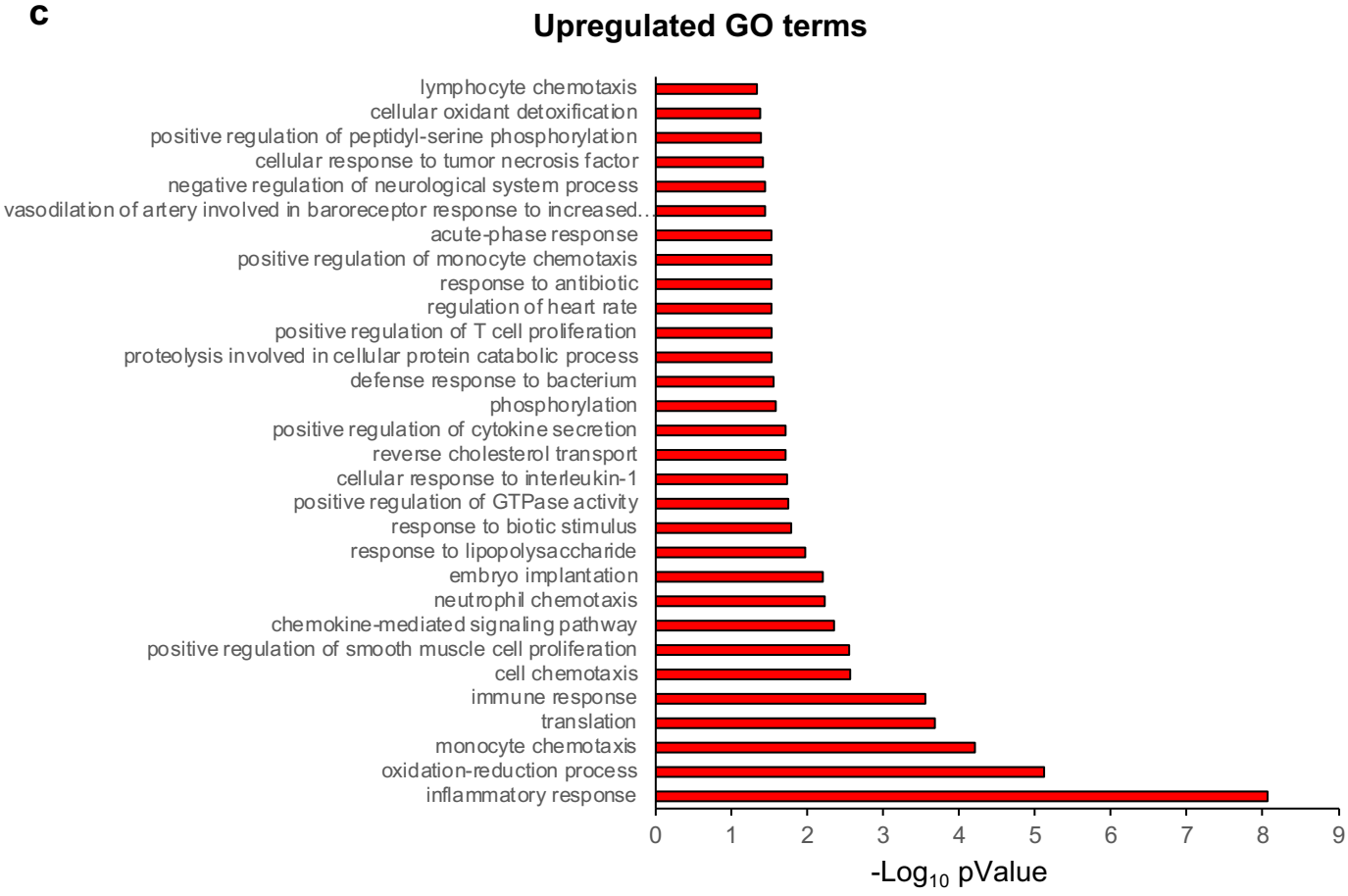
Upregulated GO terms
lymphocyte chemotaxis
cellular oxidant detoxification
positive regulation of peptidyl-serine phosphorylation
cellular response to tumor necrosis factor
negative regulation of neurological system process
vasodilation of artery involved in baroreceptor response to increased..
acute-phase response
positive regulation of monocyte chemotaxis
response to antibiotic
regulation of heart rate
positive regulation of T cell proliferation
proteolysis involved in cellular protein catabolic process
defense response to bacterium
phosphorylation
positive regulation of cytokine secretion
reverse cholesterol transport
cellular response to interleukin-1
positive regulation of GTPase activity
response to biotic stimulus
response to lipopolysaccharide
embryo implantation
neutrophil chemotaxis
chemokine-mediated signaling pathway
positive regulation of smooth muscle cell proliferation
cell chemotaxis
immune response
translation
monocyte chemotaxis
oxidation-reduction process
inflammatory response
-Log10 pValue

Figure 5

a

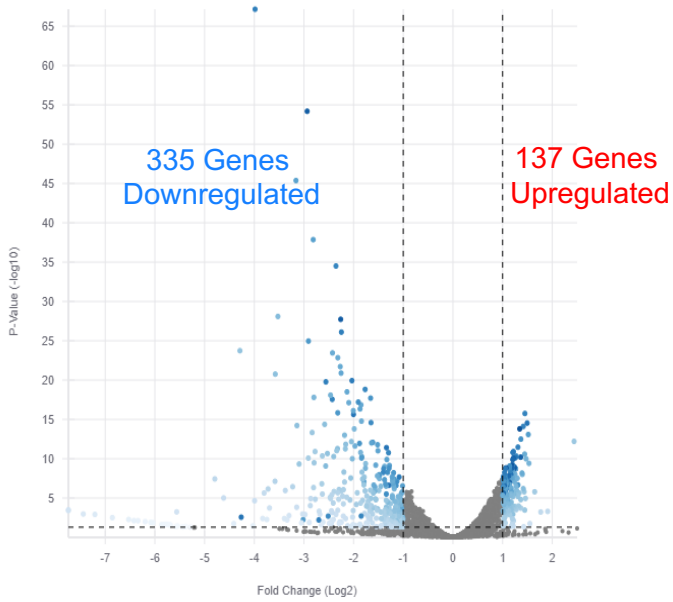
335 Genes
Downregulated
137 Genes
Upregulated
P-Value (-log10)
Fold Change (Log2)

b

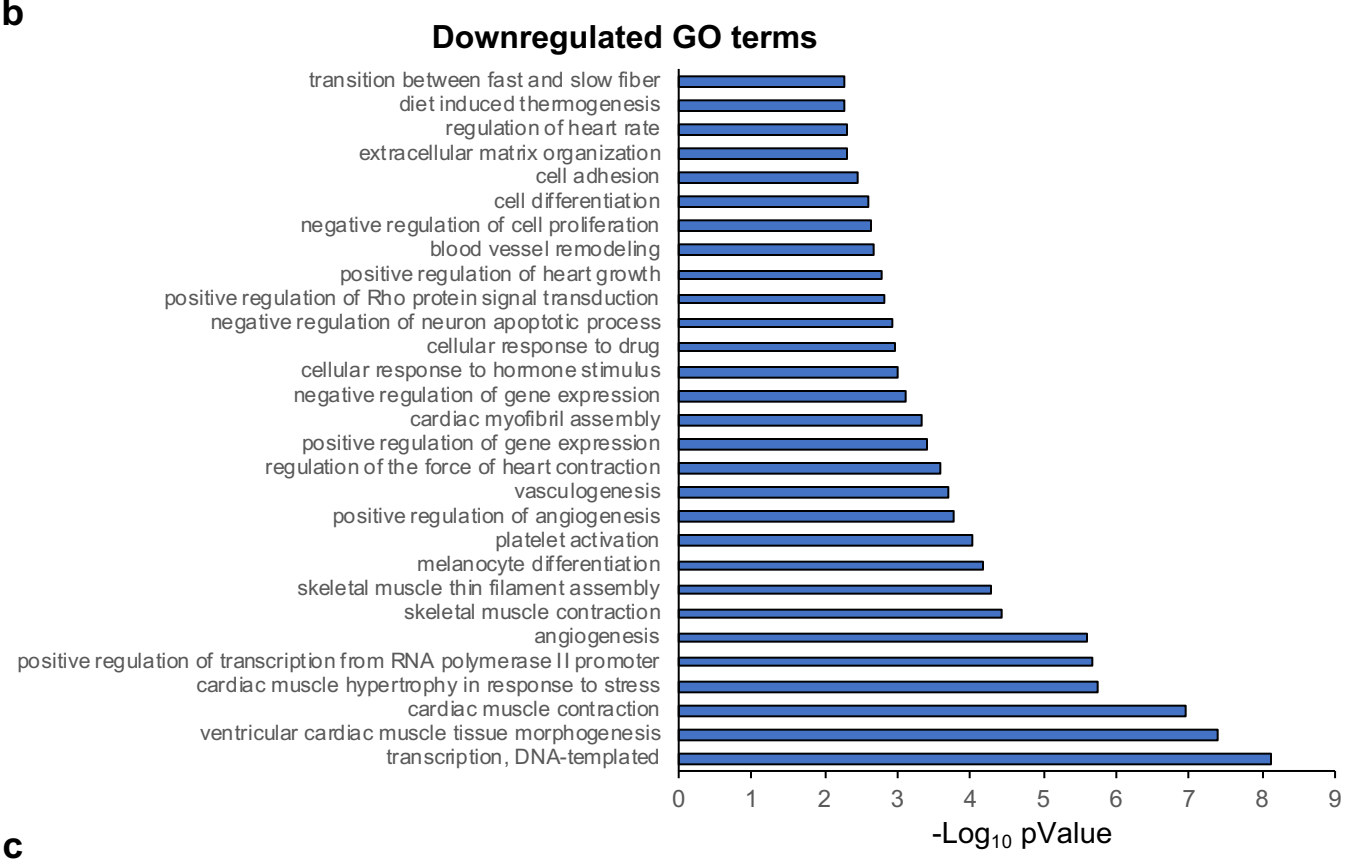
Downregulated GO terms
transition between fast and slow fiber
diet induced thermogenesis
regulation of heart rate
extracellular matrix organization
cell adhesion
cell differentiation
negative regulation of cell proliferation
blood vessel remodeling
positive regulation of heart growth
positive regulation of Rho protein signal transduction
negative regulation of neuron apoptotic process
cellular response to drug
cellular response to hormone stimulus
negative regulation of gene expression
cardiac myofibril assembly
positive regulation of gene expression
regulation of the force of heart contraction
vasculogenesis
positive regulation of angiogenesis
platelet activation
melanocyte differentiation
skeletal muscle thin filament assembly
skeletal muscle contraction
angiogenesis
positive regulation of transcription from RNA polymerase II promoter
cardiac muscle hypertrophy in response to stress
cardiac muscle contraction
ventricular cardiac muscle tissue morphogenesis
transcription, DNA-templated
-Log10 pValue

c

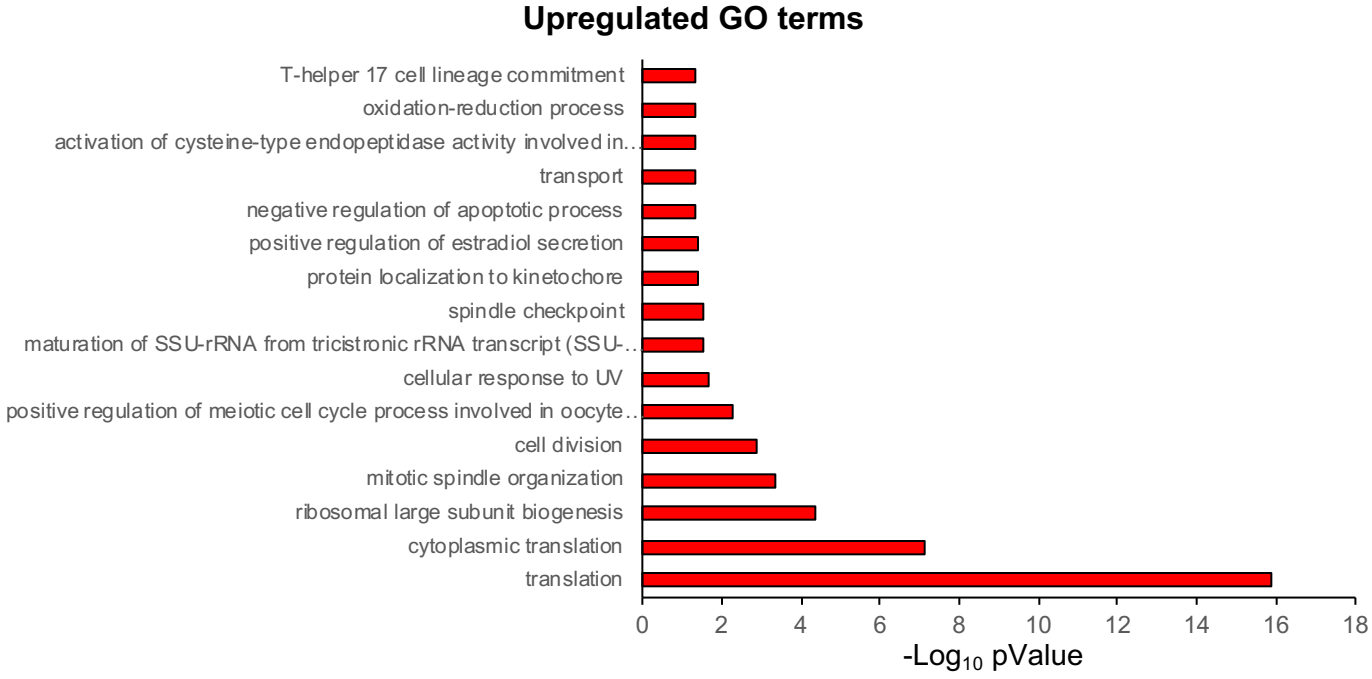
Upregulated GO terms
T-helper 17 cell lineage commitment
oxidation-reduction process
activation of cysteine-type endopeptidase activity involved in...
transport
negative regulation of apoptotic process
positive regulation of estradiol secretion
protein localization to kinetochore
spindle checkpoint
maturation of SSU-rRNA from tricistronic rRNA transcript (SSU-...
cellular response to UV
positive regulation of meiotic cell cycle process involved in oocyte...
cell division
mitotic spindle organization
ribosomal large subunit biogenesis
cytoplasmic translation
translation
-Log10 pValue

Figure 6

a

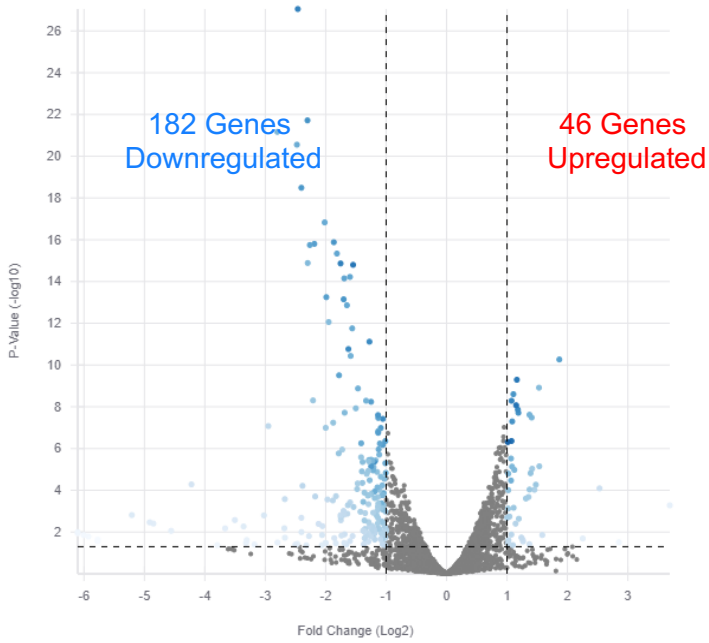
182 Genes
Downregulated
46 Genes
Upregulated
P-Value (-log10)
Fold Change (Log2)

b

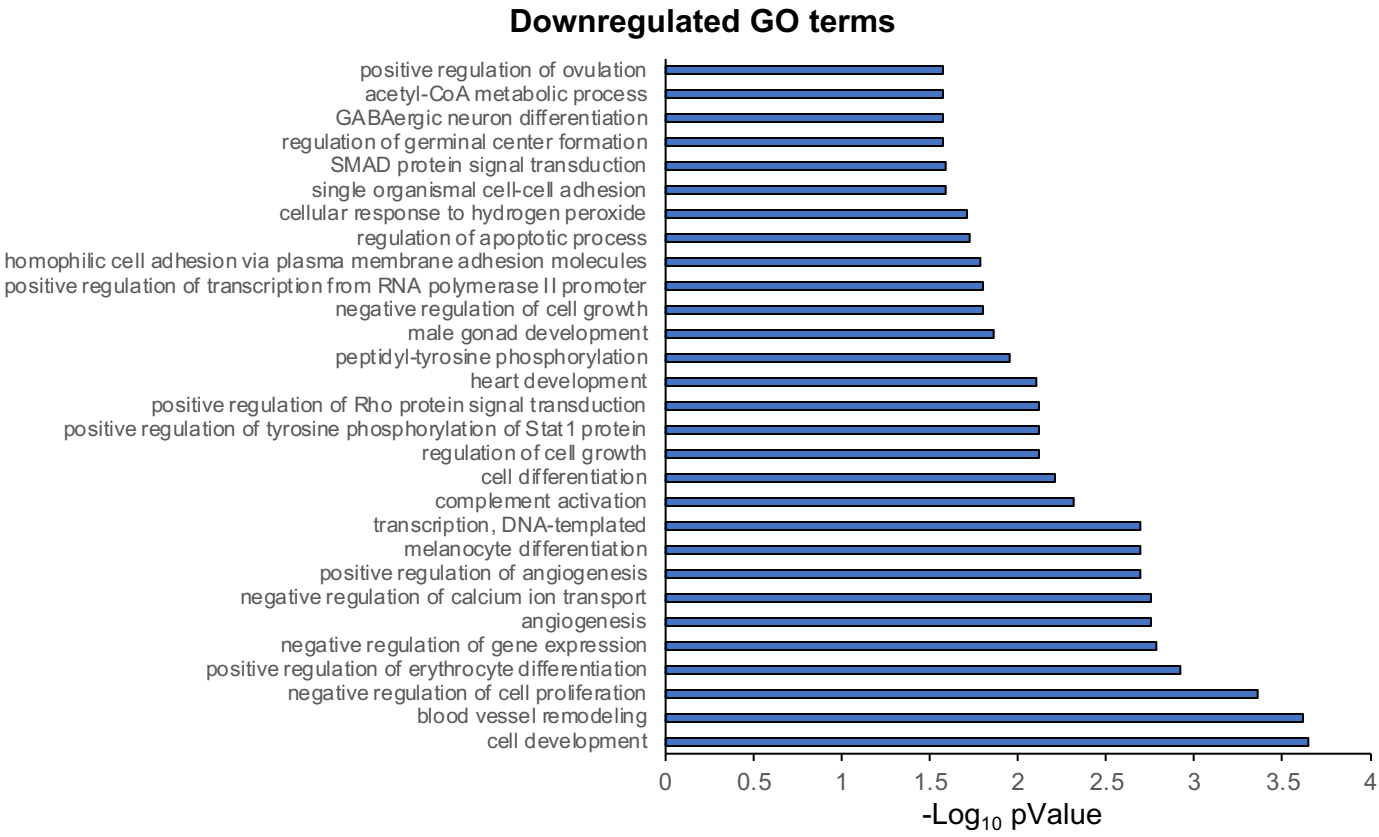
Downregulated GO terms
positive regulation of ovulation
acetyl-CoA metabolic process
GABAergic neuron differentiation
regulation of germinal center formation
SMAD protein signal transduction
single organismal cell-cell adhesion
cellular response to hydrogen peroxide
regulation of apoptotic process
homophilic cell adhesion via plasma membrane adhesion molecules
positive regulation of transcription from RNA polymerase II promoter
negative regulation of cell growth
male gonad development
peptidyl-tyrosine phosphorylation
heart development
positive regulation of Rho protein signal transduction
positive regulation of tyrosine phosphorylation of Stat1 protein
regulation of cell growth
cell differentiation
complement activation
transcription, DNA-templated
melanocyte differentiation
positive regulation of angiogenesis
negative regulation of calcium ion transport
angiogenesis
negative regulation of gene expression
positive regulation of erythrocyte differentiation
negative regulation of cell proliferation
blood vessel remodeling
cell development
-Log10 pValue

c

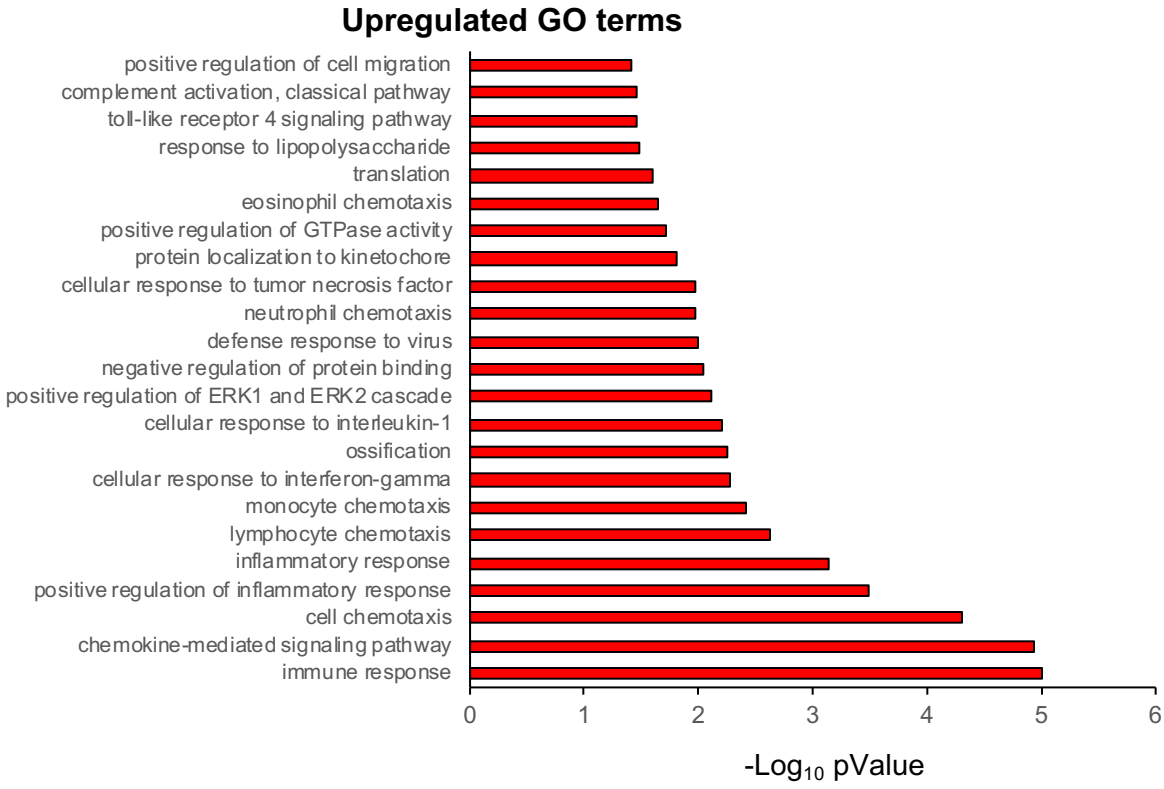
Upregulated GO terms
positive regulation of cell migration
complement activation, classical pathway
toll-like receptor 4 signaling pathway
response to lipopolysaccharide
translation
eosinophil chemotaxis
positive regulation of GTPase activity
protein localization to kinetochore
cellular response to tumor necrosis factor
neutrophil chemotaxis
defense response to virus
negative regulation of protein binding
positive regulation of ERK1 and ERK2 cascade
cellular response to interleukin-1
ossification
cellular response to interferon-gamma
monocyte chemotaxis
lymphocyte chemotaxis
inflammatory response
positive regulation of inflammatory response
cell chemotaxis
chemokine-mediated signaling pathway
immune response
-Log10 pValue

Figure 7

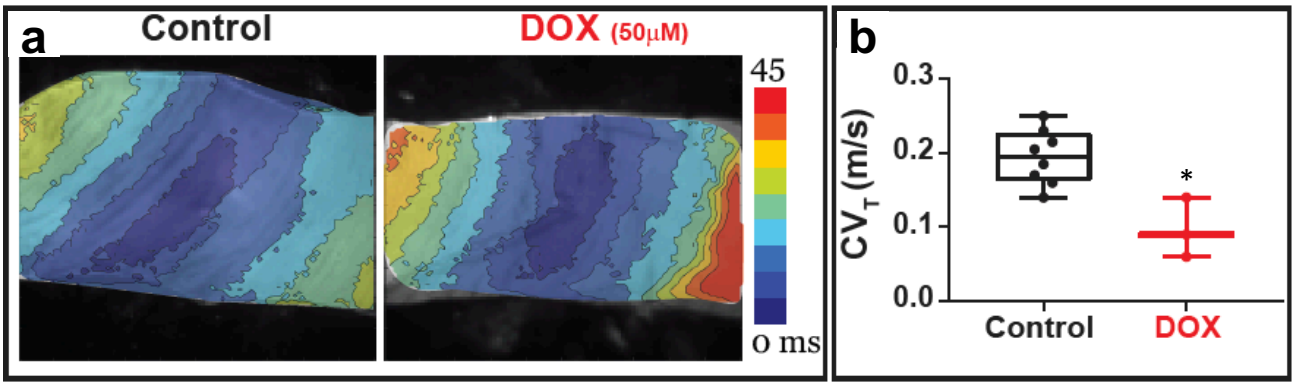
a
Control
DOX (50μM)
45
0 ms
b
0.3
0.2
0.1
0.0
CV_T (m/s)
*
Control
DOX

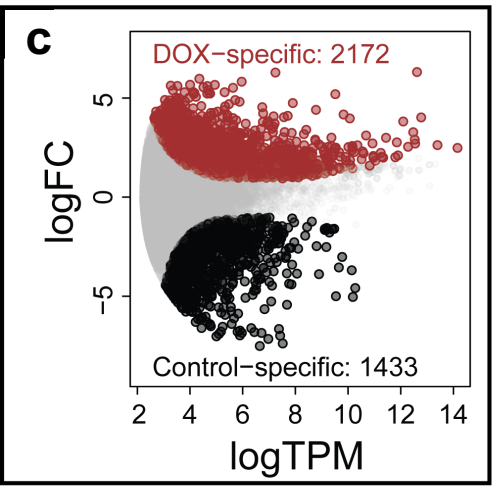
c
DOX−specific: 2172
Control−specific: 1433
logFC
5
0
−5
2
4
6
8
10
12
14
logTPM

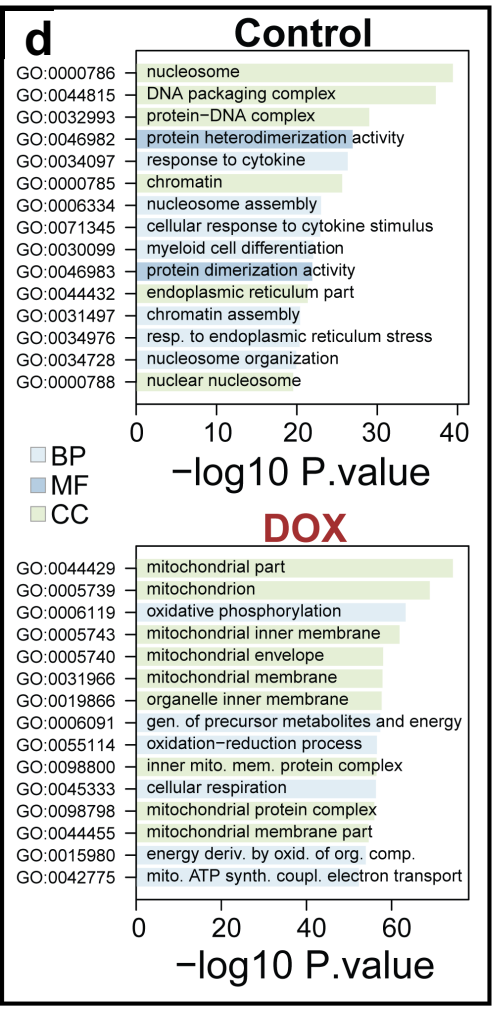
d
Control
GO:0000786 nucleosome
GO:0044815 DNA packaging complex
GO:0032993 protein−DNA complex
GO:0046982 protein heterodimerization activity
GO:0034097 response to cytokine
GO:0000785 chromatin
GO:0006334 nucleosome assembly
GO:0071345 cellular response to cytokine stimulus
GO:0030099 myeloid cell differentiation
GO:0046983 protein dimerization activity
GO:0044432 endoplasmic reticulum part
GO:0031497 chromatin assembly
GO:0034976 resp. to endoplasmic reticulum stress
GO:0034728 nucleosome organization
GO:0000788 nuclear nucleosome
0
10
20
30
40
−log10 P.value
BP
MF
CC
DOX
GO:0044429 mitochondrial part
GO:0005739 mitochondrion
GO:0006119 oxidative phosphorylation
GO:0005743 mitochondrial inner membrane
GO:0005740 mitochondrial envelope
GO:0031966 mitochondrial membrane
GO:0019866 organelle inner membrane
GO:0006091 gen. of precursor metabolites and energy
GO:0055114 oxidation−reduction process
GO:0098800 inner mito. mem. protein complex
GO:0045333 cellular respiration
GO:0098798 mitochondrial protein complex
GO:0044455 mitochondrial membrane part
GO:0015980 energy deriv. by oxid. of org. comp.
GO:0042775 mito. ATP synth. coupl. electron transport
0
20
40
60
−log10 P.value

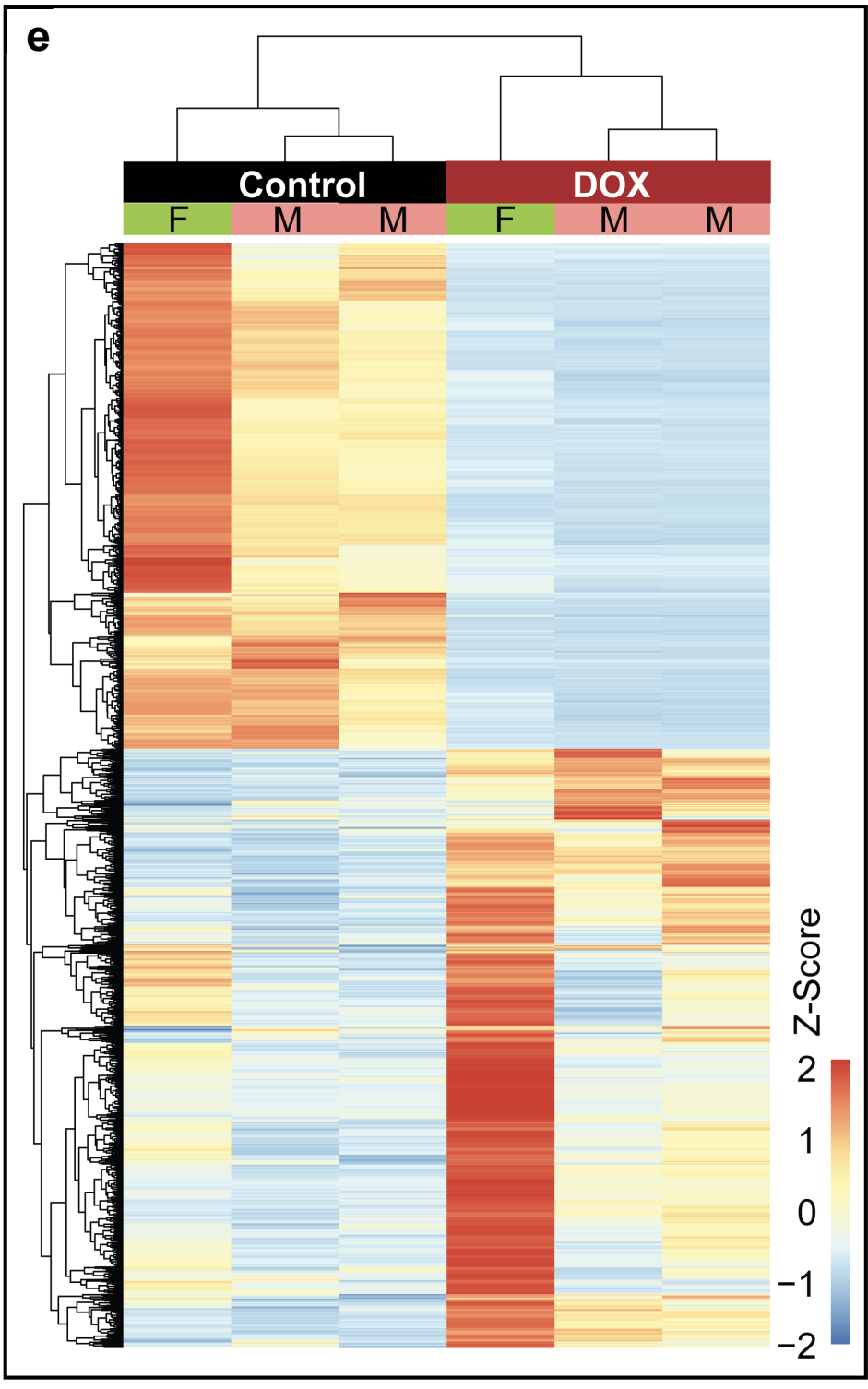
e
Control
DOX
F
M
M
F
M
M
Z-Score
2
1
0
−1
−2